PLOS BIOLOGY

RESEARCH ARTICLE

Widespread regulation of the maternal transcriptome by Nanos in *Drosophila*

Mohammad Marhabaie[¤], Tammy H. Wharton, Sung Yun Kim, Robin P. Wharton*

Department of Molecular Genetics, Department of Cancer Biology and Genetics, Center for RNA Biology, Ohio State University, Columbus, Ohio, United States of America

¤ Current address: The Steve and Cindy Rasmussen Institute for Genomic Medicine Abigail Wexner Research Institute at Nationwide Children's Hospital Columbus, Ohio, United States of America
* wharton.88@osu.edu

Citation: Marhabaie M, Wharton TH, Kim SY, Wharton RP (2024) Widespread regulation of the maternal transcriptome by Nanos in *Drosophila*. PLoS Biol 22(10): e3002840. https://doi.org/10.1371/journal.pbio.3002840

Academic Editor: Simon Bullock, MRC Laboratory of Molecular Biology, UNITED KINGDOM OF GREAT BRITAIN AND NORTHERN IRELAND

Received: October 25, 2023

Accepted: September 14, 2024

Published: October 14, 2024

Data Availability Statement: RNAseq reads are available from the Gene Expression Omnibus (GEO) under accession code GSE264028. Computer code is available at https://zenodo.org/doi/10.5281/zenodo.13337141. All other underlying data are in Supplementary Data Excel files.

Funding: This research was supported in part by NIGMS R01GM084376 (RPW). The funders had no role in study design, data collection and

Abstract

The translational repressor Nanos (Nos) regulates a single target, maternal *hunchback* (*hb)* mRNA, to govern abdominal segmentation in the early *Drosophila* embryo. Nos is recruited to sites in the 3′ UTR of *hb* mRNA in collaboration with the sequence-specific RNA-binding protein Pumilio (Pum); on its own, Nos has no binding specificity. Nos is expressed at other stages of development, but very few mRNA targets that might mediate its action at these stages have been described. Nor has it been clear whether Nos is targeted to other mRNAs in concert with Pum or via other mechanisms. In this report, we identify mRNAs targeted by Nos via 2 approaches. First, we identify mRNAs depleted upon expression of a chimera bearing Nos fused to the nonsense mediated decay (NMD) factor Upf1. We find that, in addition to *hb*, Upf1-Nos depletes approximately 2,600 mRNAs from the maternal transcriptome in early embryos. Virtually all of these appear to be targeted in a canonical, *hb*-like manner in concert with Pum. In a second, more conventional approach, we identify mRNAs that are stabilized during the maternal zygotic transition (MZT) in embryos from *nos*$^{-}$ females. Most (86%) of the 1,185 mRNAs regulated by Nos are also targeted by Upf1-Nos, validating use of the chimera. Previous work has shown that 60% of the maternal transcriptome is degraded in early embryos. We find that maternal mRNAs targeted by Upf1-Nos are hypoadenylated and inefficiently translated at the ovary–embryo transition; they are subsequently degraded in the early embryo, accounting for 59% of all destabilized maternal mRNAs. We suggest that the late ovarian burst of Nos represses a large fraction of the maternal transcriptome, priming it for later degradation by other factors in the embryo.

Introduction

Nanos (Nos) is a conserved cytoplasmic repressor that binds to mRNAs, recruiting effectors that block translation and promote degradation [1,2]. A wealth of genetic evidence reveals that Nos is primarily active in the germline, where it controls various aspects of development in a number of organisms. In *Drosophila*, mouse, and humans, Nos is required for the maintenance of germline stem cells [3–5]. Later in germline development, Nos regulates common pathways

analysis, decision to publish, or preparation of the manuscript.

Competing interests: The authors have declared that no competing interests exist.

Abbreviations: AD, activation domain; Bcd, Bicoid; BRE, Bruno Response Element; Bru, Bruno; DAPI, 4′,6-diamidino-2-phenylindole; DBD, DNA-binding domain; ES, enrichment score; FDR, false discovery rate; GSC, germline stem cell; HA, hemagglutinin; hb, *hunchback*; l(3)mbt, *lethal (3) malignant brain tumor*; LOESS, locally estimated scatterplot smoothing; MZT, maternal zygotic transition; NBS, Nanos Binding Site; NMD, nonsense mediated decay; Nos, Nanos; NRE, Nanos Response Element; NTD, N-terminal domain; PBS, phosphate-buffered saline; PBT, PBS containing 0.1% Tween-20; PGC, primordial germ cell; PRE, Pum binding site; Pum, Pumilio; RBD, RNA-binding domain; RRM, RNA recognition motif; TE, translational efficiency.

in the primordial germ cells (PGCs) of *Drosophila* [6–9] and *Caenorhabditis elegans* [10,11], including the repression of somatic gene transcription, inhibition of proliferation, and escape from apoptosis.

Evidence of a role for Nos in somatic cells is more limited. In the prospective somatic cytoplasm of the preblastoderm embryo, Nos has been thought to have 1 major regulatory target for specification of abdominal segmentation, maternal *hunchback* (*hb*) mRNA (discussed below) [12–14]. At later stages of development, Nos regulates dendritic arborization in the peripheral nervous system and the structure of the neuromuscular junction of larvae [15–17]. In other somatic tissues, a latent capacity of Nos to regulate gene expression is revealed in the absence of *lethal (3) malignant brain tumor* [*l(3)mbt*], which encodes a component of 2 transcriptional repressor complexes (dREAM and LINT). In *l(3)mbt* mutant larval brains and somatic ovarian cells, expression of Nos (and other germline-restricted genes) is derepressed; remarkably, although hundreds of transcripts are derepressed in the absence of *l(3)mbt*, mutant phenotypes in both tissues are completely suppressed by loss of Nos activity [18,19]. A similar latent regulatory capacity of Nos has been identified in cultured mammalian cells lacking dREAM activity [20]. Thus, in *Drosophila* (and likely other organisms as well), both the expression of Nos in the germline and its repression in somatic cells is important for normal development.

Given the diversity of its biological roles, it is likely that Nos regulates a number of mRNAs in various organisms. Support for such an idea comes from the Seydoux lab, who compared the maternal transcriptomes in wild-type and *nos* mutant PGCs from early *C. elegans* embryos, before the onset of zygotic transcription [10]. They found that levels of 171 maternal mRNAs are up-regulated in the absence of the redundant function of Nos-1 and Nos-2, which are required for normal development and survival of the PGCs. It is unclear how many additional maternal mRNAs are translationally repressed but not destabilized and, therefore, undetected in their experiments. Later in embryonic PGC development, 871 PGC mRNAs are up-regulated in the absence of Nos function as a result of both delayed turnover of maternal mRNAs and inappropriate zygotic transcription. Nos is not thought to directly regulate transcription and so presumably acts indirectly to stimulate accumulation of new, zygotic mRNAs.

The mechanism of Nos-dependent regulation is best understood for repression of maternal *hb* mRNA in *Drosophila*. On its own, Nos binds with high affinity but no detectable sequence specificity to RNA [21,22]; however, in collaboration with Pumilio (Pum), it is recruited specifically to composite binding sites (Nanos Response Elements; NREs) in the *hb* mRNA 3′ UTR [22,23]. The composite sites have the consensus sequence $\frac{U}{A}\frac{U}{A}\frac{U}{A}$ UGUA, with Nos recognizing the first 3 degenerate positions (i.e., the Nanos Binding Site; NBS) and Pum the next 4. Within the Pum/Nos/RNA ternary complex, amino acid interactions along a protein–protein interface mediate conformational changes in both proteins that enhance binding. A key component of the interface is the Nos C-terminal tail, which is essential for RNA binding; 7 amino acids in the tail of the Nos^{L7} mutant protein are absent, and as a result, it is not recruited into a ternary complex and does not regulate *hb* mRNA in the embryo [22–24].

Despite an atomic-level understanding of Nos recruitment to the *hb* NRE, 2 outstanding questions about Nos activity in *Drosophila* remain. First, how many mRNAs does *Drosophila* Nos regulate in addition to *hb* (and the handful referenced above)? And second, is Nos recruited to other regulatory targets via its C-terminal tail in collaboration with Pum, as has generally been assumed; or do other RNA-binding proteins recruit Nos via a different mechanism? If Nos bound to a long, information-rich sequence that were rigidly constrained, analysis of the transcriptome sequence might be sufficient to identify likely regulatory targets. But the consensus NRE has low information content and mutations in the NBS portion of the

NRE have only a modest effect on activity in vivo [25]. So even though 6,225 3′ UTRs in the total *Drosophila* transcriptome bear one or more consensus NREs [26], it is unclear whether these are genuine regulatory targets in vivo.

To address these issues, we first attempted to identify mRNAs that copurify with Nos, a method that has been used successfully to identify Pum targets, for example [27,28]. Initial reconstruction experiments revealed a disappointingly small enrichment of *hb* mRNA. We therefore turned to an unconventional approach, expressing in flies a chimeric protein with the nonsense mediated decay (NMD) factor Upf1 fused to Nos. Early work on NMD showed that tethering Upf1 via an exogenous RNA-binding domain (RBD) to reporter mRNAs could direct their degradation [29,30]; we reasoned that tethering Upf1 to mRNAs via Nos might lead to their degradation and that Nos regulatory targets would be depleted from the transcriptome in RNAseq experiments.

Results

As shown in Fig 1A, Nos is expressed at 4 important stages of oogenesis and early embryogenesis [24,31,32]: (1) in the germline stem cells (GSCs), where it is required for maintenance of stem cell status; (2) in a high-level burst at stage 10B in the nurse cells just prior to a general shutdown of transcription as the egg chamber nears maturation; (3) during oogenesis stages 13 to 14 and continuing during syncytial nuclear cleavage cycles 1 to 9 in a gradient emanating from the posterior pole of the embryo, where it represses translation of maternal *hb* mRNA; and (4) at nuclear cycle 10 in the PGCs, where it regulates proliferation, blocks apoptosis, and is required for migration into the somatic gonad much later in embryogenesis. After division of the GSC, expression of Nos is turned off in the differentiating daughter cell (the cystoblast) and subsequently reexpressed at various stages of oogenesis. No role has been ascribed to Nos in these stages of oogenesis, including the burst at stage 10B.

Expression of Upf1-Nos inhibits activity of the anterior determinants Hb and Bicoid (Bcd) and causes the degradation of *bcd* mRNA

With the goal of identifying mRNA regulatory targets of Nos, we prepared transgenic flies that express either a Upf1-Nos chimera, or one of 3 control proteins: Upf1; Nos; or Upf1-Nos^{L7}, which bears the C-terminal tail deletion that abrogates recruitment to *hb* mRNA. Transcription of each transgene is dependent on the GAL4 driver that is introduced by appropriate crosses, and each transgenic mRNA bears the 3′ UTR of wild-type *nos* mRNA to provide the posttranscriptional regulation conferred on native *nos*.

We first drove expression of Upf1-Nos and the 3 control proteins described above with Nos GAL4-VP16, which directs transcription in the germarium and subsequent stages of oogenesis. Females expressing Upf1-Nos produce essentially no eggs and bear rudimentary ovaries; in contrast, females expressing Upf1, Nos, or Upf1-Nos^{L7} appear to produce normal numbers of eggs. As explained in more detail below, we wished to harvest eggs at nuclear cycle 9 to take advantage of the prolonged transcriptional quiescence flanking the oocyte–egg transition (Fig 1A) and therefore asked whether use of another GAL4 driver would permit egg development. We found this to be the case with a maternal *alpha*Tub>GAL4 driver, which directs expression throughout much of oogenesis and was used in all subsequent experiments. To determine the extent to which Upf1-Nos is overexpressed relative to endogenous Nos, we prepared transgenes encoding HA-epitope tagged versions of each protein. Expression of Upf1-HA-Nos was driven by the *alpha*Tub>GAL4 driver referred to above; expression of HA-Nos was under the control of native signals in an otherwise wild-type fragment of genomic DNA that rescues the *nos* mutant phenotype. Comparison of the level of maternally derived protein in 0- to 2-hour

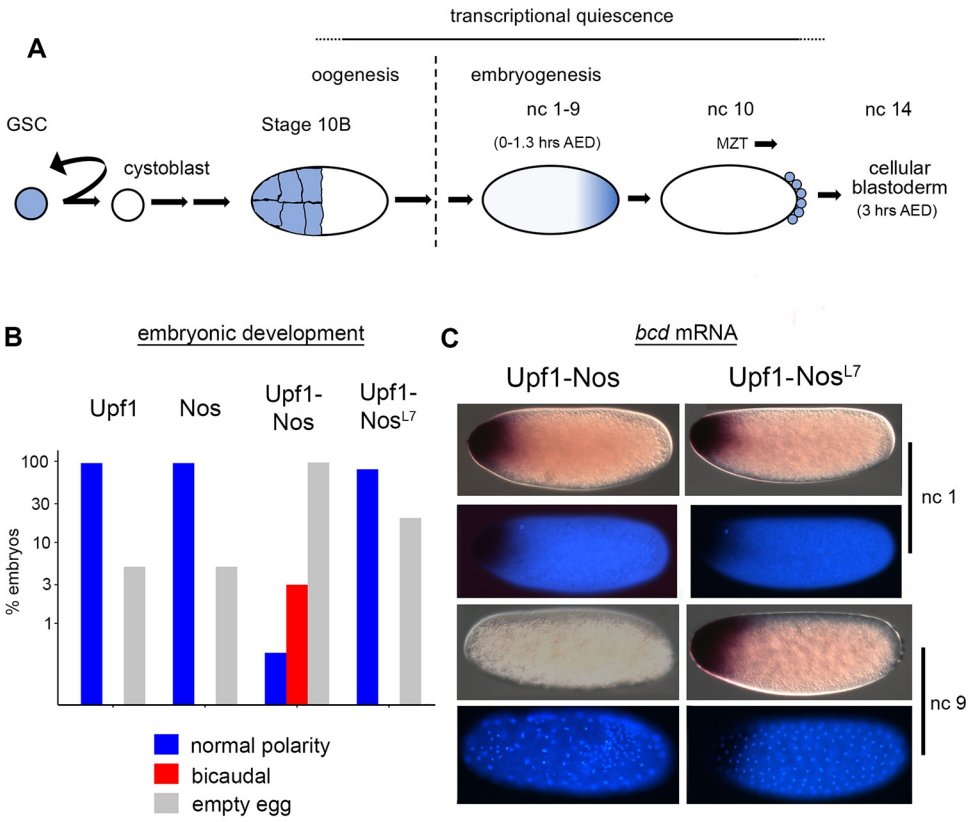

Fig 1. Upf1-Nos suppresses activity of anterior determinants *bcd* and *hb*. (**A**) Timeline of Nos expression during oogenesis and early embryogenesis, focusing on 4 developmental stages. As indicated, nc 1–9 take place in the first 1.3 hours of development AED. Subsequent nuclear divisions are considerably slower: nc 13–14 occur 2–3 hours AED, culminating in formation of the cellular blastoderm. The approximately 10-hour period of transcriptional quiescence preceding harvesting of mRNA samples for subsequent analysis (noted above) ends in the MZT, which takes place in several waves, with the onset of transcription beginning in nc 10. (**B**) Embryonic phenotypes resulting from maternal expression of the 4 regulatory proteins, as indicated. For the bar graph (note the logarithmic y-axis), embryos were aged ≥24 hours (allowing wild type to hatch) and then scored by sorting into 3 bins: cuticle with normal polarity (either hatched or not), cuticle with anterior polarity inversion and a bicaudal body plan, or no cuticle (empty egg), which includes both unfertilized eggs and embryos that die prematurely. Underlying data are in S1 Data. (**C**) The distribution of *bcd* mRNA in Upf1-Nos and Upf1-Nos^{L7} embryos at 2 different stages of early embryogenesis—nc 1 in the first 2 rows and nc 9 in the second 2 rows. At each stage, 2 micrographs of a single embryo are shown, using Nomarski optics to visualize *bcd* mRNA and morphology (above), and fluorescence methods to visualize DAPI-stained DNA (below). Statistical analysis is reported in S1 Data. Note that Upf1-Nos embryos appear to be unusually fragile during the fixation for in situ hybridization; many are lost on the wall of the glass tube or at the heptane/aqueous interface. AED, after egg deposition; *bcd*, *bicoid*; GSC, germline stem cell; *hb*, *hunchback*; MZT, maternal zygotic transition; nc, nuclear cycle; Nos, Nanos.

https://doi.org/10.1371/journal.pbio.3002840.g001

embryonic extracts reveals that Upf1-Nos is overexpressed approximately 3-fold (S1 Fig and S1 Data).

Although females expressing Upf1-Nos lay eggs, virtually none hatch. In a pilot study, 0/245 Upf1-Nos eggs hatched, whereas between 80% and 95% of Upf1, Nos, or Upf1-Nos^{L7} control eggs hatched. Since expression of Upf1-Nos is exclusively maternal, we expected that defects might be evident early in embryonic development. Therefore we harvested 0- to 3-hour-old embryos and examined the distribution of nuclei by staining with DAPI to assess developmental progress. Unlike the 3 control genotypes, a large fraction of Upf1-Nos embryos have a single nucleus and are either not fertilized or fail to commence nuclear division cycles; we have not investigated this further and restricted subsequent analysis to fertilized embryos

between nuclear cycles 2 to 13. Almost all the Upf1, Nos, and Upf1-Nos^{L7} embryos exhibit normal distributions of syncytial cleavage stage nuclei (94% to 100%; see S1 Data for details). In contrast, 63% of Upf1-Nos embryos have abnormal nuclear distributions, with irregularly spaced nuclei and variable DNA content, based on the intensity of DAPI fluorescence (e.g., Fig 1C).

We next asked whether the Upf1-Nos embryos that fail to hatch exhibit interpretable developmental defects by examining their body plan, as revealed by pattern in the epidermal cuticle secreted late in embryonic development. About 97% of Upf1-Nos eggs were "empty," without detectable cuticle, probably because they die earlier in development (Fig 1B). However, among the 3% of Upf1-Nos embryos that did secrete cuticle, 2 had normal segmentation and 14 revealed a striking bicaudal body plan, in which normal head and thoracic segments are replaced by a mirror image duplication of posterior abdominal segments (Fig 1B). Bicaudal development is diagnostic for simultaneous inhibition of Bcd and Hb activity [33–35]. None (0/862) of the Upf1, Nos, or Upf1-Nos^{L7} control embryos exhibited segmental polarity reversals, much less a mirror image duplication of the abdomen. As shown in Fig 1B, most (80% to 95%) of the control embryos secreted cuticle that revealed body plans with normal antero-posterior polarity and, at most, minor defects; the remaining embryos failed to secrete cuticle.

Even though only a few Upf1-Nos exhibited bicaudal body plans, the phenotype is sufficiently characteristic to strongly suggest that Upf1-Nos inhibits activity of both Hb and Bcd. *bcd* is transcribed exclusively maternally, while *hb* is transcribed both maternally and, later, zygotically (under the control of Bcd). For simplicity, we therefore focused on examining the effects of Upf1-Nos on *bcd* mRNA by in situ hybridization in early cleavage stage embryos. Most (82%) of the Upf1-Nos embryos that were either unfertilized or in the first nuclear division cycles have a normal level of *bcd* mRNA at the anterior (Fig 1C); this was also the case for most (95%) control Upf1-Nos^{L7} embryos in cycles 0 to 2. But we observed a novel phenotype in Upf1-Nos embryos that we judged to be approximately in cycles 9 to 10 based on nuclear density: an absence of detectable *bcd* mRNA (Fig 1C). In contrast, Upf1-Nos^{L7} embryos in cycles 9 to 10 have normal levels and distributions of *bcd* mRNA at the anterior pole.

In summary, the vast majority of control Upf1, Nos, and Upf1-Nos^{L7} embryos develop normally, which is consistent with subsequent analysis of their transcriptomes (below). In contrast, Upf1-Nos embryos are abnormal: Many fail to either fertilize or commence nuclear division, subsequent nuclear divisions are abnormal, only a handful escape the deleterious early effects of Upf1-Nos and progress through to late development, and none hatch. Most importantly, 2 phenotypes—the absence of *bcd* mRNA during early development and the bicaudal body plan of Upf1-Nos embryos—support our premise that the chimeric protein would degrade Nos-regulated mRNAs.

Upf1-Nos depletes 39% of maternal mRNAs

To identify targets of Upf1-Nos in the entire transcriptome, we prepared triplicate samples from 4 experimental genotypes (Upf1, Nos, Upf1-Nos, and Upf1-Nos^{L7}) as well as wild-type embryos as a control. Embryo collections were soft-fixed in methanol, stained with DAPI, and manually sorted in the fluorescence stereomicroscope to identify embryos at nuclear cycle 9 to 10, or in the case of Upf1-Nos, embryos that appeared to be approximately the same age despite an abnormal distribution of nuclei (as in Fig 1C). Because transcription in the germ line ceases at stage 10B of oogenesis and resumes only during the MZT beginning at nuclear cycle 10, preexisting Upf1-Nos (or the other ectopically expressed regulators) in the collected embryos have had the opportunity to act on the maternal transcriptome for approximately 9

to 10 hours without synthesis of new mRNA. Prior to the transcriptional "shutoff," Upf1-Nos might cause changes to the transcriptome via both direct and indirect mechanisms; we hoped that direct action of Upf1-Nos during the period of transcriptional quiescence would have a predominant effect on transcriptome composition in embryos harvested at nuclear cycle 9. RNA was prepared from all the genotypes, prepared for RNAseq, and analyzed by standard methods.

We first assessed the quality of our samples. The absence of detectable mRNAs encoded by genes that comprise the first zygotic response to maternal patterning gradients (e.g., *Kr*, *gt*, *kni*) supports the idea that embryos were in fact collected prior to the MZT (see S2 Data). Reducing the complexity of all 15 samples by Multidimensional Scaling reveals that biological replicates are similar to each other and that the control samples are also similar to each other (S2 Fig). In contrast, the Upf1-Nos samples are markedly different from all 3 UAS controls and wild type, consistent with their unusual embryonic phenotypes (Fig 1).

We next compared the transcriptomes of each experimental genotype to wild type to identify genes with altered expression, arbitrarily setting a minimum 2-fold threshold change and a false discovery rate (FDR) < 0.05. For simplicity, we describe data in which all mRNA isoforms for a gene are binned; analysis of individual mRNA isoforms yields broadly similar results (S3 Fig). We initially found that a small fraction of the maternal transcriptome is depleted (2.4%) or enriched (2.1%) upon expression of Upf1 alone (Fig 2A). Because we were interested primarily in mRNAs that are targeted by the Nos portion of the Upf1-Nos chimera, we excluded Upf1-regulated genes from subsequent analysis of Upf1-Nos and Upf1-Nos^{L7}.

As shown in Fig 2A, the expression of Upf1, Nos, or Upf1-Nos^{L7} has relatively little effect on the transcriptome. The proportion of significantly up- and down-regulated genes is approximately the same for Upf1 and Nos, and the proportion of the transcriptome depleted by Upf1-Nos^{L7} is only modestly greater than the proportion of up-regulated genes. In contrast, preliminary analysis of mRNAs in Upf1-Nos embryos suggested that many mRNAs were significantly down-regulated (S4 Fig). The large, asymmetric effect of Upf1-Nos on the transcriptome results in oversampling of nontargeted mRNAs. To account for this effect, we adjusted the normalization factors of Upf1-Nos samples in analyzing differential expression using an average derived from 20 highly expressed mRNAs (most of which encode ribosomal proteins), on the assumption they are not differentially expressed (as described [36]). Subsequent analysis reveals that >39% (n = 2,596) of the genes encoding maternal mRNAs are depleted more than 2-fold by Upf1-Nos (Fig 2A).

To test the normalization described above and obtain an independent measure of changes in abundance due to expression of Upf1-Nos, we measured the levels of 16 mRNAs by quantitative reverse transcription PCR (RT-qPCR); these were chosen to span a $\log_2 = 15$-fold change in abundance. As shown in Fig 2B, the 2 methods show excellent agreement, with a Pearson's correlation R value of 0.98. The absence of a significant population of enriched mRNAs in the Upf1-Nos data supports a premise of our experiment—that tethering Upf1 to mRNAs via Nos during the transcriptionally quiescent period preceding sample collection would lead to their degradation via NMD and that this degradation would predominate to shape the composition of the transcriptome. We assume that indirect effects (i.e., up-regulation of some mRNAs as a secondary consequence of the action of Upf1-Nos on other, directly targeted mRNAs) are minimized in the absence of concurrent transcription.

Several observations support the idea that, although Upf1-Nos targets a large portion of the transcriptome, it does so specifically. First, the inactivity of Upf1-Nos^{L7} argues that the wild-type chimera acts in collaboration with Pum to specifically target NRE-bearing mRNAs, a point we return to in the following section. Second, 3 of the 4 mRNAs previously shown to be bound and regulated by Nos—*hb*, *bcd*, and *alpha-Importin* [37,38]—are targeted by Upf1-Nos;

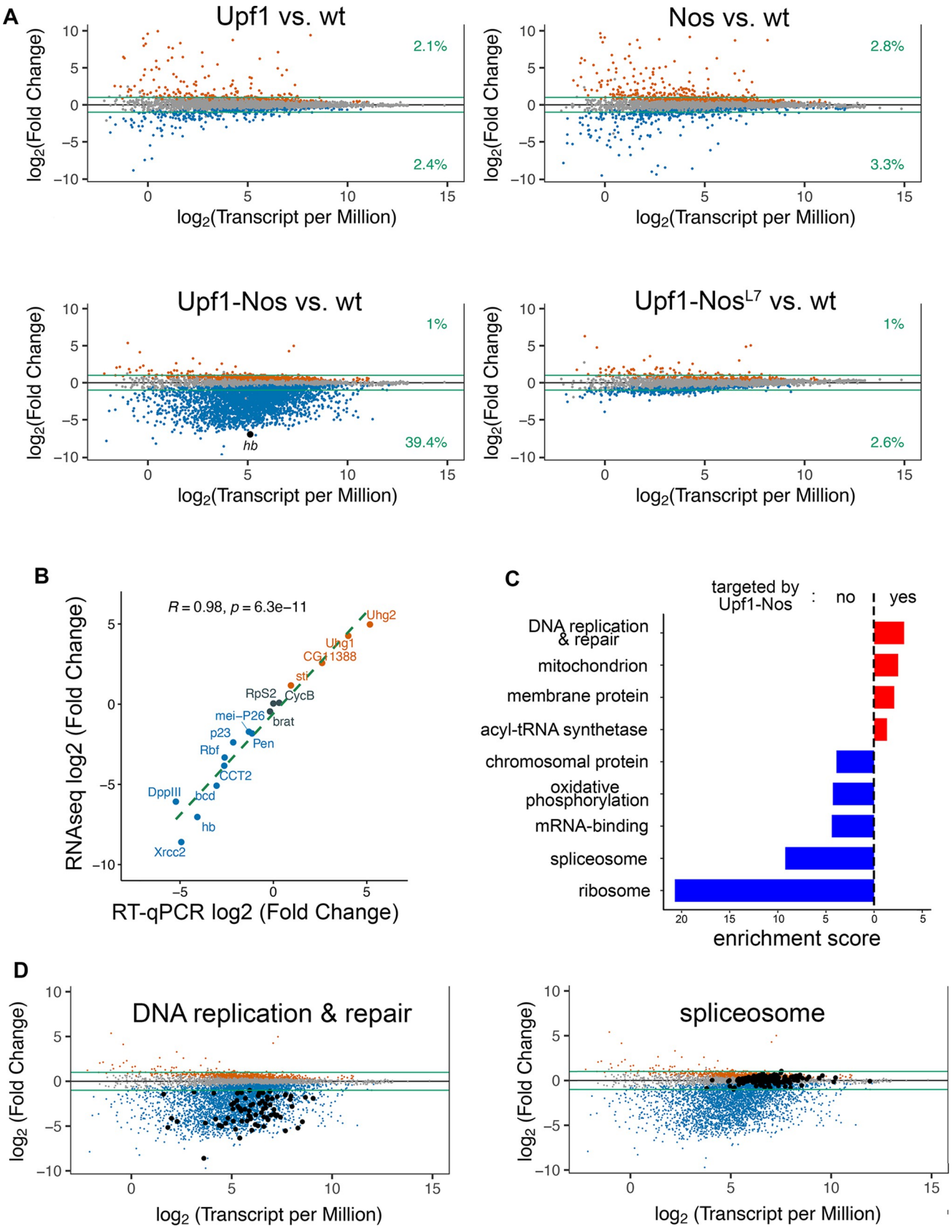
A
Upf1 vs. wt
Nos vs. wt
Upf1-Nos vs. wt
Upf1-Nos^{L7} vs. wt
log2(Fold Change)
log2(Transcript per Million)
2.1%
2.4%
2.8%
3.3%
1%
39.4%
hb
1%
2.6%
B
R = 0.98, p = 6.3e−11
RNAseq log2 (Fold Change)
RT-qPCR log2 (Fold Change)
Uhg2
Uhg1
CG11388
stl
RpS2
CycB
mei−P26
brat
p23
Pen
Rbf
CCT2
DppIII
bcd
hb
Xrcc2
C
targeted by Upf1-Nos
no
yes
DNA replication & repair
mitochondrion
membrane protein
acyl-tRNA synthetase
chromosomal protein
oxidative phosphorylation
mRNA-binding
spliceosome
ribosome
enrichment score
D
DNA replication & repair
spliceosome
log2 (Fold Change)
log2 (Transcript per Million)

Fig 2. Upf1-Nos targets a large fraction of the maternal transcriptome. (**A**) For each of the misexpressed proteins, the plot shows the difference in mRNA abundance in comparison to wt (log_2 fold change) as a function of the average mRNA abundance (log_2 transcripts per million reads) for embryonic samples collected at nc 9–10. Each dot represents a binned collection of mRNA isoforms for a single gene; analysis of individual isoforms is in S3 Fig. Genes altered by expression of Upf1 are excluded from the analysis of Upf1-Nos and Upf1-Nos^{L7} data. Gene-binned mRNAs significantly depleted and enriched are indicated in blue and orange, respectively. The green lines mark $log_2 \pm 1$, and the numbers at the right indicate the fraction of the (gene-binned) transcriptome that is significantly changed and above or below the arbitrary 2-fold cutoff. *hb* is highlighted in the Upf1-Nos plot. (**B**) Correlation between the difference in mRNA abundance (Upf1-Nos vs. wt) measured by RNAseq and by RT-qPCR for a collection of genes, which span an approximately 1,000-fold range in expression level in wt. (**C**) The results of DAVID analysis reveal gene sets enriched among Upf1-Nos-targeted mRNAs (red) and nontargeted mRNAs (blue), which are plotted vs. their ES. Shown are annotation clusters with highest ES for which at least 1 Category has a Benjamini adjusted p-value < 0.05. For clarity, 3 clusters that satisfy these criteria and are enriched among nontargeted mRNAs with ES between 2.3 and 1.9 were omitted (see S2 Data for details). (**D**) Examples of enriched gene sets, highlighted on the Upf1-Nos vs. wt plot from (A). Underlying data for the figure are in S2 Data. ES, enrichment score; *hb*, *hunchback*; nc, nuclear cycle; Nos, Nanos; RT-qPCR, quantitative reverse transcription PCR; wt, wild type.

https://doi.org/10.1371/journal.pbio.3002840.g002

moreover, *hb*, which is the critical Nos target in the early embryo, is one of the most highly depleted mRNAs (highlighted in Fig 2A). The exception is *CycB* mRNA, which is bound by Nos in collaboration with Pum and repressed in the PGCs [1,7], but not targeted by Upf1-Nos. (We note that, for reasons that are not clear, Nos is necessary but not sufficient to repress most of the *CycB* mRNA in these experiments, which derives from the prospective somatic cytoplasm [1].) Third, if Upf1-Nos acted promiscuously, due to high nonspecific binding (for example), it would preferentially target mRNAs with longer 3′ UTRs; in fact, mRNAs targeted by Upf1-Nos have on average slightly shorter 3′ UTRs than nontargeted mRNAs (S5 Fig).

The depletion of such a large fraction of the transcriptome by Upf1-Nos suggests that Nos regulates thousands of mRNAs in *Drosophila*, in contrast to the hundreds regulated by Nos in *C. elegans* [10]. Since such a large fraction of the transcriptome is targeted by Upf1-Nos, it is unclear whether it is meaningful to identify preferentially targeted pathways. Nevertheless, clustering analysis of gene function via DAVID [39,40] reveals that a number of pathways are significantly enriched among the pool of genes targeted by Upf1-Nos as well as the pool of untargeted genes (Fig 2C). Among Upf1-Nos targeted genes, only 4 clusters have gene subsets with significant Benjamini-adjusted p-values; the most highly enriched of these subsets encodes factors involved in DNA replication and repair (enrichment score [ES] = 3.1; Fig 2C), perhaps accounting for the aberrant replication seen in Upf1-Nos embryos (Fig 1C). An independent search for *Drosophila* genes associated with the Gene Ontology terms "DNA replication" and "DNA repair" revealed that 79/79 are depleted, as shown in Fig 2D. Among genes not targeted by Upf1-Nos, constituents of the ribosome (ES = 20.7) and spliceosome (ES = 9.2) are even more significantly enriched (Fig 2C and 2D). We conclude that while Upf1-Nos selectively targets a few biological processes/pathways with modest preference, it acts globally to deplete maternal mRNAs that encode factors distributed across most biological functions.

Upf1-Nos acts primarily in conjunction with Pum

Three lines of evidence support the idea that, in targeting a large fraction of the maternal transcriptome, Upf1-Nos acts in collaboration with Pum, much as native Nos and Pum collaboratively repress *hb* mRNA.

First, Upf1-Nos^{L7} is almost inert, changing the transcriptome to essentially the same minor extent as does Upf1 (Fig 2A). The C-terminal tail of Nos that is altered in the L7 mutant is specifically required to promote cooperative binding of Pum and Nos to the NREs in *hb* mRNA.

Second, a set of 538 ovarian mRNAs that copurify with affinity-tagged Pum [27] is enriched among mRNAs depleted by Upf1-Nos (p-value = 0.03 by the CAMERA competitive test of [41]; Fig 3A).

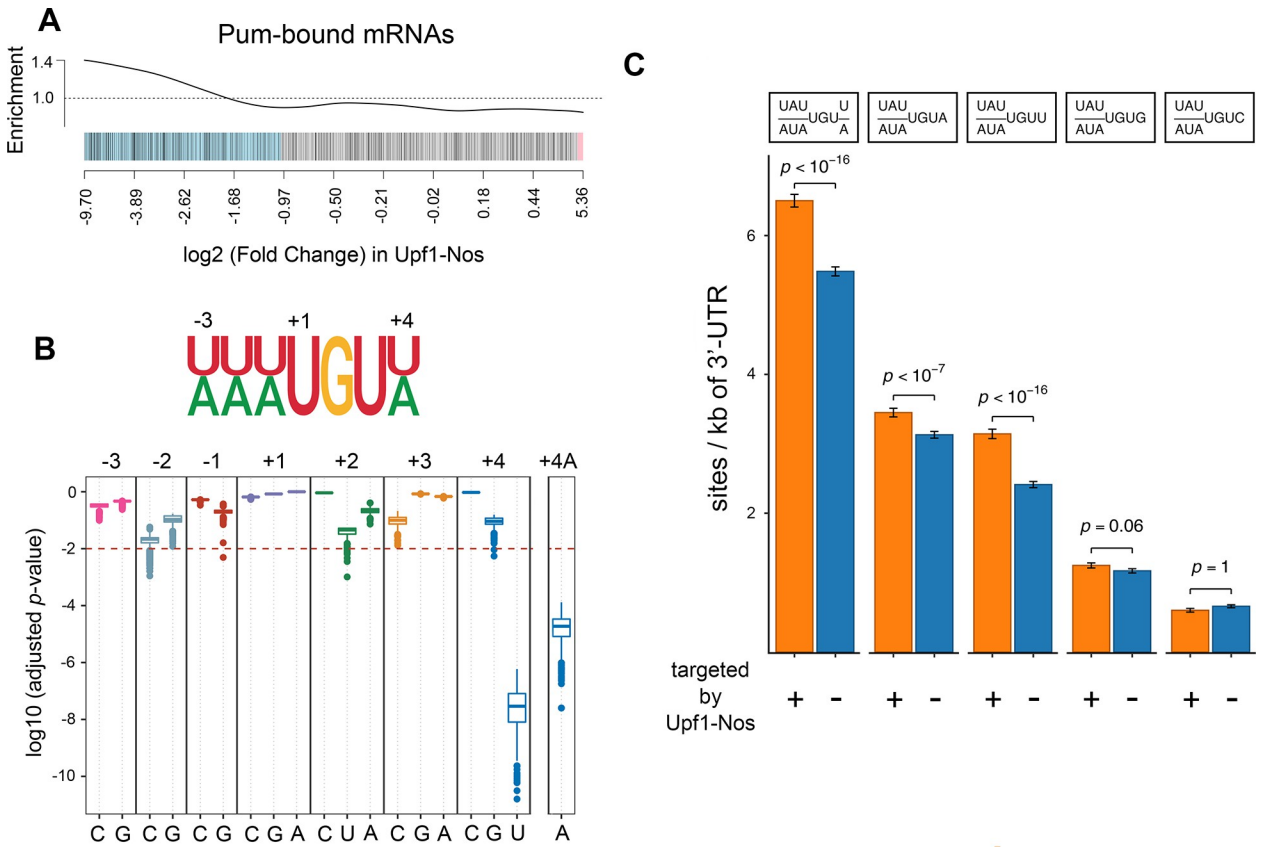

Fig 3. Pum mediates most of the activity of Upf1-Nos. (**A**) Barcode plot showing enrichment among mRNAs depleted by Upf1-Nos of mRNAs bound by transgene-encoded Pum RNA-binding domain in ovarian extracts identified by Gerber and colleagues [27]. Each mRNA is represented by a line; mRNAs depleted and enriched > $\log_2 = 1$ are highlighted in blue and red, respectively. Here and in subsequent barcode analyses, the x-axis is nonlinear. (**B**) A modified NRE motif (shown above) is enriched among the 3′ UTR sequences of mRNAs depleted by Upf1-Nos. The plot below is of adjusted *p*-values (Hommel) for the significance of the enrichment on the y-axis of each possible motif variant displayed along the x-axis; enrichment of the canonical NRE motif (e.g., +4A) is shown to the right. Enrichment was calculated as described in the text, and each boxplot displays the distribution of *p*-values from 1,000 trial comparisons between the fraction of 3′ UTRs bearing ≥1 motif in targeted vs. nontargeted mRNAs. (**C**) Bar graph showing mean number of various sites (shown above) per kb of 3′ UTR in targeted and nontargeted mRNAs, with error bars representing the SEM. The first pair of columns on the left shows enrichment of the modified NRE motif, and subsequent columns show enrichment of variants at position +4 of this motif, with *p*-values calculated in the Wilcoxon test. The data are also displayed by local regression in S6 Fig. Underlying data for the figure are in S2 Data. Pum, Pumilio; Nos, Nanos; NRE, Nanos Response Element.

https://doi.org/10.1371/journal.pbio.3002840.g003

Third, the 3′ UTRs of mRNAs targeted by Upf1-Nos are enriched for a modified Nos+Pum binding motif, $\frac{U}{A}\frac{U}{A}\frac{U}{A}$ UGU $\frac{U}{A}$, in which position +4 is either U or A. This enrichment emerged from 2 analyses.

First, we asked whether the canonical Nos+Pum motif ($\frac{U}{A}\frac{U}{A}\frac{U}{A}$ UGUA) is enriched among 3′ UTRs targeted by Upf1-Nos, comparing the fraction of 3′ UTRs bearing the motif between randomly selected subsets of targeted and nontargeted mRNAs, chosen to have the same number of sequences and similar distributions of 3′ UTR lengths. As shown at the right of Fig 3B, the fraction of targeted 3′ UTRs bearing at least 1 canonical site (with A at position +4) is significantly greater than the fraction of nontargeted UTRs (median *p*-value of 1,000 trials = 1.9×10^{-5}). As controls, we asked whether singly substituted mutant derivatives at each of the 7 motif positions are also enriched. All of the derivatives but one appear to be "mutant" sites not significantly enriched in targeted 3′ UTRs; the exception is $\frac{U}{A}\frac{U}{A}\frac{U}{A}$ UGUU, which, in fact, is enriched to a greater extent than the canonical site (Fig 3B).

Second, we measured the density of Nos+Pum motifs, comparing 3′ UTR sequences from mRNAs targeted and not-targeted by Upf1-Nos. As shown in Figs 3C and S6, the average number of $\frac{U}{A}\frac{U}{A}\frac{U}{A}$ UGU $\frac{U}{A}$ sites is significantly enriched in targeted mRNAs, unlike $\frac{U}{A}\frac{U}{A}\frac{U}{A}$ UGUG or $\frac{U}{A}\frac{U}{A}\frac{U}{A}$ UGUC sites (Fig 3C). The results shown in Fig 3B and 3C are consistent with work described elsewhere showing that Nos+Pum bind efficiently to NREs with either U or A at position +4 [42].

Taken together, the evidence described above supports the idea that Upf1-Nos is primarily recruited to its targets by Pum in a manner similar to their joint recruitment to the *hb* NRE. We were unable to test Pum dependence directly, as *pum* mutant flies that also express Upf1-Nos are subviable, and females produce very few eggs.

Upf1-Nos may be recruited to a minor fraction of its targets by Bruno

Although Upf1-Nos^{L7} is largely inactive (as described above), a small cohort of 178 genes is depleted >2-fold upon expression of this mutant chimera. We find no significant enrichment of NREs in the 3′ UTR sequences of mRNAs targeted by Upf1-Nos^{L7} (Figs 4A and S7, p-value = 0.087 by Wilcoxon test). Thus, depletion is unlikely to be the result of inefficient recruitment of the mutant Nos moeity to NREs via Pum. We therefore considered the possibility that another RNA-binding protein might recruit Upf1-Nos^{L7} to this minor fraction of the transcriptome.

To identify such a putative novel Nos cofactor, we used the DREME tool [44] to search for motifs overrepresented among 3′ UTR sequences of mRNAs depleted by Upf1-Nos^{L7}. The search revealed enrichment of the motif UAU $\frac{A}{U}$ U $\frac{G}{A}$ UA, which is similar to one of the binding sites for Bruno (Bru): the Bruno Response Element (BRE) U $\frac{A}{G}$ U $\frac{G}{A}$ U $\frac{A}{G}$ U [45]. The average density of BREs is greater in mRNAs depleted ≥2-fold by Upf1-Nos^{L7} (Figs 4A and S7).

Bru is a translational repressor that binds a number of RNA motifs via its 3 RNA recognition motifs (RRMs) [46]. mRNA regulatory targets of Bru in the ovary have been identified by virtue of increased polysome association following RNAi-mediated inhibition of Bru expression [43]. If Bru mediates the depletion of mRNAs by Upf1-Nos^{L7} in our experiments, we would expect significant overlap with the Bru-regulated mRNAs identified by Rangan and colleagues. This is indeed the case: mRNAs depleted by Upf1-Nos^{L7} are enriched for Bru-regulated targets (p-value = 7.2×10^{-6}, CAMERA competitive test), as revealed in a barcode enrichment plot (Fig 4B). Functional clustering of gene analysis reveals a number of enriched gene sets among Upf1-Nos^{L7} targets; these encode membrane cytoskeleton factors or regulators (PDZ, SH3, pleckstrin domain proteins, spectrin repeat proteins), at least one of which (β-spectrin) plays a key role in GSCs and differentiation of their progeny (Fig 4C and S3 Data).

We next asked whether Bru can recruit Nos and Nos^{L7} to RNA. Previous experiments have shown that Nos and Bru proteins interact [47,48]. To further characterize the Bru–Nos interaction, we performed yeast 2-hybrid experiments, the results of which are shown in Fig 4D. We find that a fragment of Bru interacts with full-length Nos, stimulating LacZ reporter activity to a slightly greater extent than does interaction with either of 2 known Nos effectors, Cup and NOT4 (Fig 4D, above) [1,49]. In reciprocal experiments with DNA-binding domain (DBD) and transcriptional activation domain (AD) fusions swapped, we observe binding of both Nos and Nos^{L7} to Bru, demonstrating that the Bru–Nos interaction does not depend on an intact Nos C-terminal tail. Consistent with this observation, Bru interacts with the Nos N-terminal domain (NTD) but not its C-terminal RBD (Fig 4D, below).

To directly test whether RNA-bound Bru can recruit Nos to RNA, we next used yeast 3-hybrid RNA-binding experiments to show that Bru binds specifically to a synthetic RNA sequence with 3 copies of the canonical BRE, but not to RNAs with either 3 copies of a mutant BRE or 2 copies of a NRE (Fig 4E). Then, in yeast 4-hybrid experiments similar to those used

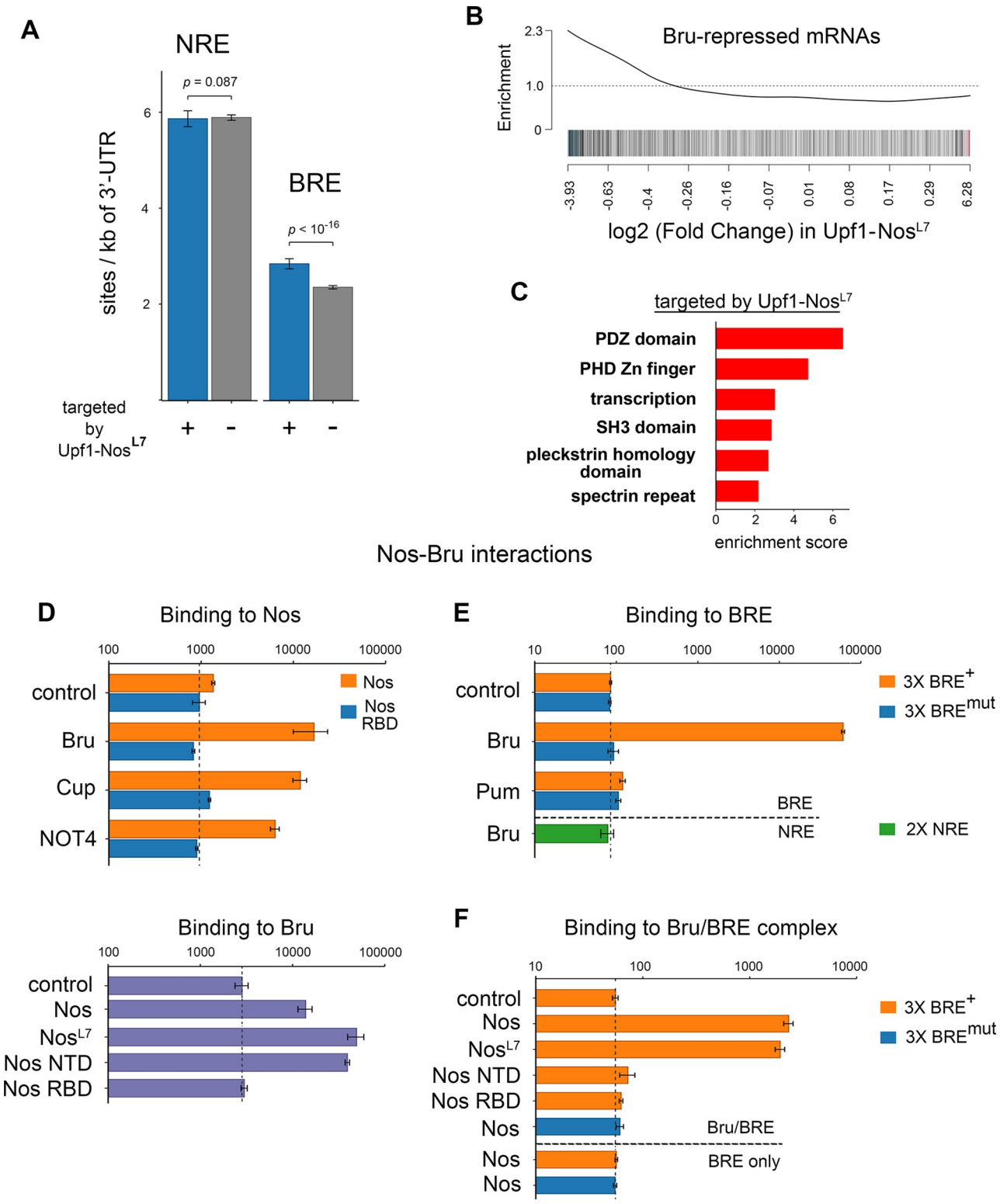

Fig 4. Upf1-Nos targets a small portion of the transcriptome via Bru. (**A**) Similar to Fig 3C, the mean 3′ UTR density of NRE and BRE sites is compared between mRNAs targeted vs. not-targeted by Upf1-Nos^{L7} (*p*-values calculated via Wilcoxon test). The data are also displayed by local regression in S7 Fig. (**B**) Barcode enrichment plot displaying mRNAs derepressed upon inhibition of Bru expression in the ovary [43] plotted vs. the $\log_2$ (fold change) in Upf1-Nos^{L7} vs. wt (e.g., Fig 2A). (**C**) DAVID analysis reveals enrichment of gene sets among mRNAs targeted by Upf1-Nos^{L7}. (**D**-**F**) Yeast interaction assays show that both Nos and Nos^{L7} can be recruited to RNA-bound Bru. In each panel, the binding of AD fusions to various

factors (y-axis) to a DNA-bound bait (title above each bar graph) is measured in arbitrary light units of β-galactosidase (x-axis, $\log_{10}$ plot). For the "control" entry in each bar graph, yeast were transformed with plasmids that express the bait indicated in the title and an empty vector encoding AD only; the background level of β-galactosidase is also indicated with a vertical dashed line. (**D**) Two-hybrid experiments showing protein–protein interactions between Nos and Bru (above) and Bru and Nos (below). We are unable to assess interaction with DBD fused to the Nos NTD, as the resulting fusion "autoactivates" transcription of the reporter without an AD-fusion partner. (**E**) Three-hybrid experiments showing specific binding of Bru to RNA bearing wt BREs. Below the horizontal dashed line is an additional control showing no significant binding of Bru to NREs. (**F**) Four-hybrid experiments showing binding of Nos and Nos^{L7} to Bru-bound RNA. Below the horizontal dashed line are additional controls showing no binding of Nos in the absence of Bru to RNA bearing either wt or mutant BREs. Note that the background level of β-galactosidase is higher in the yeast strain used for 2-hybrid experiments than in the strain used for 3- and 4-hybrid experiments. Underlying data for the figure are in S3 Data. AD, activation domain; BRE, Bruno Response Element; Bru, Bruno; DBD, DNA-binding domain; Nos, Nanos; NRE, Nanos Response Element; NTD, N-terminal domain; wt, wild type.

https://doi.org/10.1371/journal.pbio.3002840.g004

to show Pum-dependent recruitment of Nos to NREs [23], we find that RNA-bound Bru can recruit either Nos or Nos^{L7} to the RNA (Fig 4F). Recruitment is dependent on both the NTD and RBD of Nos, raising the possibility that protein–protein interactions between Bru and Nos as well as protein–RNA interactions between Nos and the RNA are required for formation of the ternary Bru/Nos/RNA complex.

Although we initially identified Bru as a mediator of the activity of Upf1-Nos^{L7}, the interaction experiments in Fig 4D–4F show that Bru interacts similarly with the L7 mutant and wild-type Nos proteins. It therefore seems likely that Bru mediates targeting of the same small subset of mRNAs by both Upf1-Nos^{L7} and Upf1-Nos but that Pum-mediated targeting of the much larger set of mRNAs by the latter obscures the contribution by Bru. Consistent with this idea, neither BREs (p-value = 0.129 by Wilcoxon test) nor Bru-repressed mRNAs (p-value = 0.084 by CAMERA competitive test; S8 Fig) are enriched among mRNAs targeted by Upf1-Nos.

In summary, we have shown that Bru can recruit Nos or Nos^{L7} to specific RNA sequences, supporting the idea that Bru mediates targeting of a minor subset of the maternal transcriptome by Upf1-Nos^{L7} (and presumably contributing to depletion of the same minor subset by Upf1-Nos). The mechanism by which the Nos-Bru-BRE complex forms is independent of the integrity of the Nos C-terminal tail and thus different from cooperative binding of Nos+Pum to the *hb* NRE.

mRNAs targeted by Upf1-Nos in transgenic animals are repressed in wild-type ovaries and embryos by Nos

We next asked whether mRNAs depleted by Upf1-Nos might be regulated by endogenous Nos in wild-type animals. As a first step to addressing this question, we reanalyzed 2 studies of maternal mRNAs in late oogenesis and early embryogenesis, partitioning these into mRNAs either targeted or not targeted by Upf1-Nos.

In the first study, Tadros and colleagues [50] identified maternal mRNAs that are degraded in unfertilized eggs; by definition, the regulation they observed occurs in the absence of zygotic gene expression. Tadros and colleagues [50] identified 1,069 mRNAs whose abundance drops at least 1.5-fold as unfertilized eggs age. This set of destabilized maternal mRNAs is significantly enriched among our Upf1-Nos targets (p-value = 1.6×10^{-11}; Fig 5A). The embryos used in their experiments were unfertilized but otherwise wild type, and, therefore, destabilization must be mediated by endogenous maternal factors.

In the second study, Eichhorn and colleagues [51] characterized mRNAs in staged samples from wild-type ovarian egg chambers and timed embryo collections up to 6 hours after egg deposition, measuring abundance, poly(A) tail length, and translational efficiency (TE). Their work reveals comprehensive changes to the maternal transcriptome during an extended span of development that includes the oocyte–egg transition (e.g., the vertical dashed line in Fig 1A) and the MZT, a period from approximately 1.5 to 3.0 hours of embryonic development during

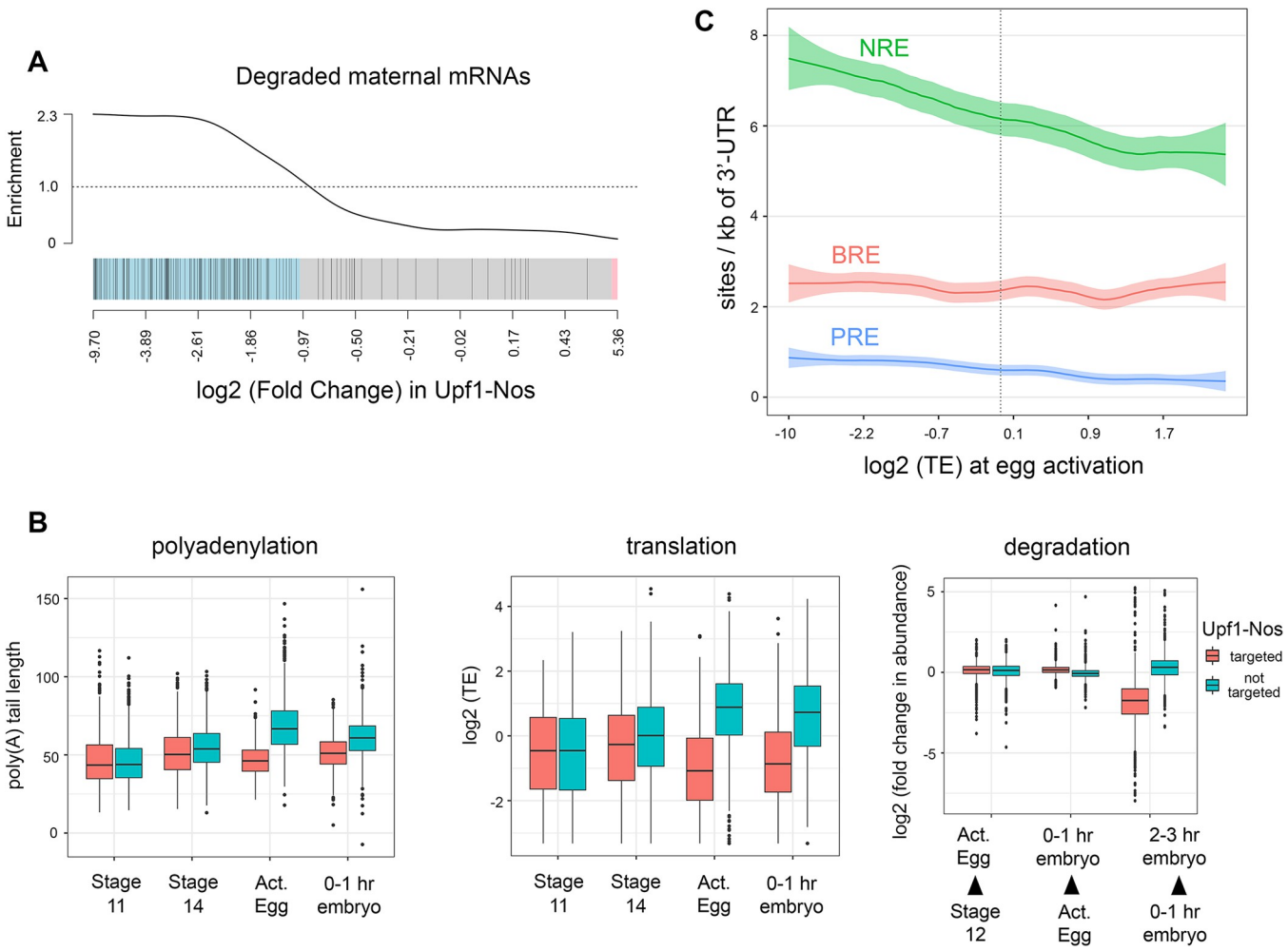

Fig 5. Maternal mRNAs targeted by Upf1-Nos are translationally repressed and degraded in wild-type eggs. (**A**) Barcode plot displaying enrichment of maternal mRNAs degraded in unfertilized eggs [50] vs. $\log_2$ (fold change) in Upf1-Nos vs. wt (e.g., Fig 2A). (**B**) Maternal mRNAs expressed at nc 9–10 in the RNAseq experiments of Fig 2 were binned into those targeted (red) and not targeted (teal) by Upf1-Nos. Then, the poly(A) tail length and relative translational efficiency of each mRNA was extracted from the data of Eichhorn and colleagues [51] at the 4 stages of development indicated below: stage 11 and 14 oocytes, activated eggs, 0–1-hour embryos (before the onset of zygotic transcription). The plot at the right is of the change in abundance for each maternal mRNA between each of the 3 developmental transitions indicated below, again using the data of Eichorn et al. (2016). Statistical analysis in S4 Data. Note that zygotic transcription contributes significantly to mRNA abundance in the 2–3-hour embryo pool, but all other time points analyze purely maternal mRNAs. (**C**) Local regression analysis of binding motifs in mRNA 3′ UTRs as a function of TE at egg activation, from the data of Eichorn et al. (2016). For this analysis, we chose the most highly expressed maternal isoform for each gene. Underlying data for the figure are in S4 Data. nc, nuclear cycle; Nos, Nanos; TE, translational efficiency; wt, wild type.

https://doi.org/10.1371/journal.pbio.3002840.g005

which many maternal mRNAs are degraded and zygotic transcription is activated. Analyzing their data, we find that mRNAs targeted by Upf1-Nos are regulated differently than are non-targeted mRNAs. Nontargeted maternal mRNAs undergo lengthening of their poly(A) tails at egg activation and concomitant enhanced translation, consistent with the observation that poly(A) tail length and TE are coupled until the onset of gastrulation (which occurs at 3 hours of embryonic development) [51]. In contrast, Upf1-Nos targets undergo neither poly(A) tail lengthening nor translational enhancement (Fig 5B). The repressed Upf1-Nos targets are stable until embryogenesis but degraded between the 0- to 1- and 2- to 3-hour windows of development (Fig 5B). The data likely underestimate the extent of degradation during the MZT, since some maternally transcribed mRNAs are retranscribed zygotically, as discussed below.

Taken together, the data in Fig 5 suggest that, late in oogenesis, the large set of approximately 2,600 mRNAs targeted by Upf1-Nos (in transgenic animals) is translationally repressed in wild-type animals during late oogenesis and subsequently degraded in the early embryo. We suggest that these regulatory events are a delayed response to the burst of Nos expression that peaks at stage 10B of oogenesis (Fig 1A), which represses targeted mRNAs and primes them for subsequent degradation in the embryo.

As a first test of the idea that Nos is responsible for repressing a large cohort of maternal mRNAs, we asked whether the modified NRE motif that mediates Nos+Pum binding is overrepresented among maternal mRNAs that are translated inefficiently at egg activation. As shown in Fig 5C, localized regression analysis reveals a correlation between the translational efficiency and the density of modified NRE motifs in the 3′ UTR across the maternal transcriptome. In comparison with the 3′ UTRs of mRNAs that are not repressed, the modified NRE is enriched in the 3′ UTRs of repressed mRNAs (defined as TE < 1, p-value $= 1.1 \times 10^{-8}$ by two-sided Wilcoxon test). As controls, canonical Pum binding sites (PREs) and BREs are present at lower density (Figs 5C and S9) and are enriched to a lesser extent (PREs) or not at all (BREs) in repressed mRNAs (p-values of 7.3×10^{-6} and 0.22, respectively).

All the work described above is based on the ectopic expression of Upf1-Nos, which behaves like a hyperactive version of Nos that efficiently degrades bound mRNAs. Part of the rationale for using Upf1-Nos is that, in the *Drosophila* embryo, Nos acts primarily to block translation and only secondarily to promote the degradation of targeted mRNAs [35,37,52,53]. In *C. elegans*, RNAseq analysis of *nos* mutant PGCs successfully identified a cohort of maternal mRNAs that are destabilized by Nos in wild-type PGCs [10]. This observation led us to ask (1) if we could detect Nos-dependent destabilization of maternal mRNAs and (2) whether the same mRNAs are targeted by Upf1-Nos and by Nos. To address these issues, we collected embryos from wild-type and nos^{-} females at 0 to 1 and 2 to 3 hours of development (i.e., before and after the onset of zygotic transcription, respectively) and measured the abundance of maternal mRNAs via RNAseq. In analyzing the data, we ignored mRNAs that are transcribed zygotically, but not maternally, since these are not exposed to and thus cannot be regulated by Nos.

As shown in Fig 6A, at 0 to 1 hours of development, the wild-type and nos^{-} mRNA populations are similar in composition, with only 3.5% of the maternal transcriptome significantly enriched $>\log_2 = 0.5$-fold in nos^{-} embryos. A somewhat greater fraction of the maternal transcriptome (5.6%) is depleted in nos^{-} embryos at this stage of development, presumably due to indirect effects of Nos on gene expression earlier, during ovarian development (since Nos is thought to act primarily as a repressor). However, after the onset of the MZT, 18.5% of the maternal transcriptome is stabilized in 2- to 3-hour nos^{-} embryos (Fig 6A). We have not examined where in embryos Nos-dependent degradation takes place; however, we note that 35% of targeted maternal mRNAs are up-regulated >2-fold in the absence of Nos, suggesting that in wild-type animals, it acts throughout the cytoplasm rather than just in the posterior, as in the case of maternal *hb*. A rank-ordered barcode display of mRNAs stabilized in the absence of Nos reveals a correlation with mRNAs targeted by Upf1-Nos (p-value $= 3.8 \times 10^{-14}$; Fig 6B). In fact, 86% (1,019/1,185) of the mRNAs stabilized in the absence of Nos are depleted by Upf1-Nos (Fig 6C). Taken together, the complementary loss- and gain-of-function results of Figs 6 and 2 indicate that Nos regulates at least these 1,019 common mRNA targets.

What then of the 1,528 maternal mRNAs that are regulated by Upf1-Nos but apparently not by Nos (Fig 6C)? One possibility is that they are repressed but not degraded by Nos. Another possibility is that they are repressed and degraded by Nos and then reexpressed zygotically during the 2- to 3-hour window of embryonic development. At this stage, Nos is confined to the PGCs (which constitute only a small fraction of the volume of the embryo), and,

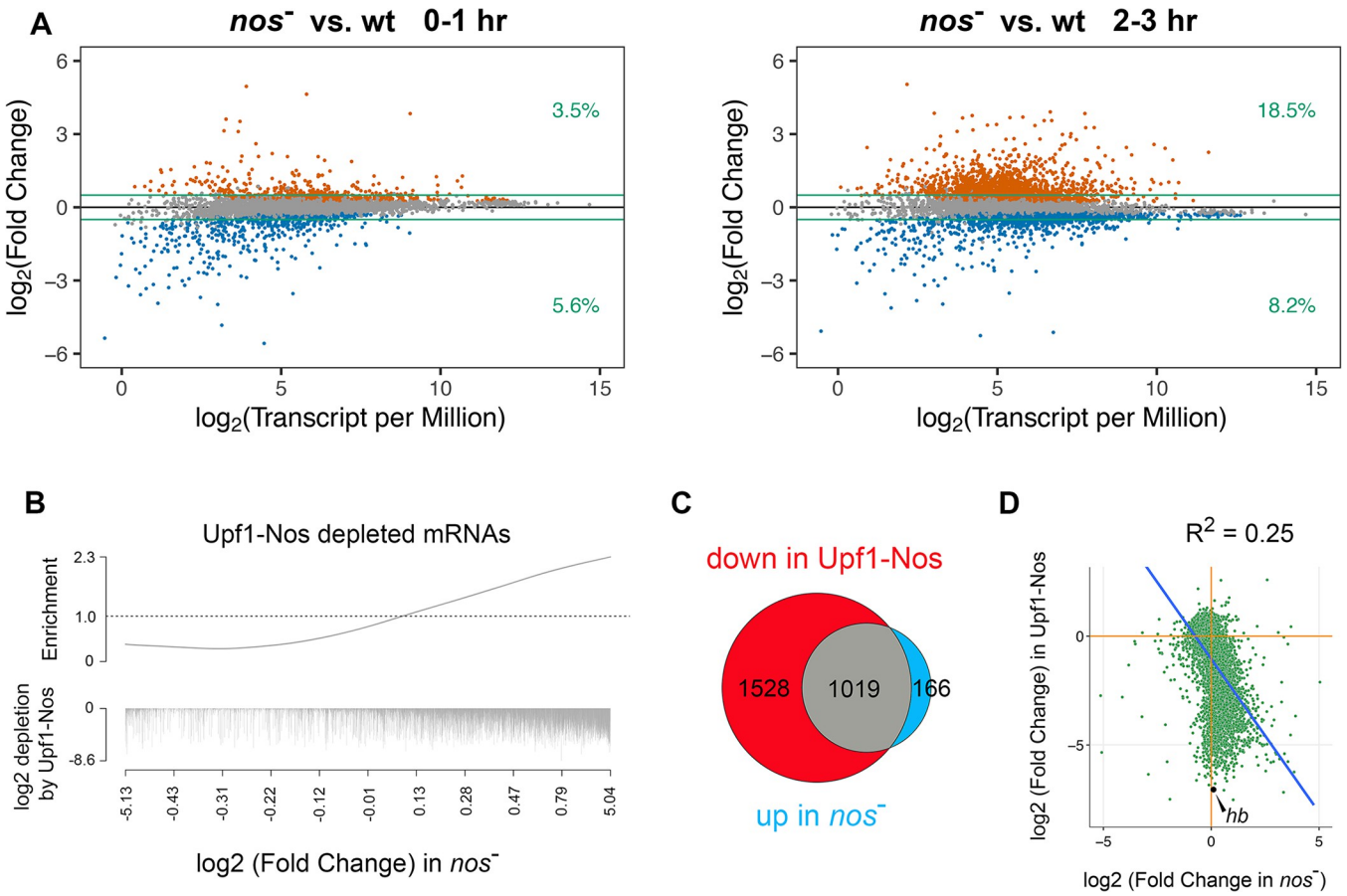

Fig 6. Regulation of maternal mRNA abundance by endogenous Nos in wild-type oocytes and embryos. (**A**) Results of RNAseq analysis, comparing the abundance of maternal mRNAs between wild-type and *nos*⁻ embryos at 0–1 and 2–3 hours of embryonic development. Only maternal mRNAs (based on the manually sorted embryos used in the RNAseq experiments of Fig 2 are shown. The green lines mark $\log_2 \pm 0.5$, and the figures at the right indicate the fraction of the (gene-binned) transcriptome that is significantly changed and above or below the arbitrary cutoff, which is smaller than the 2-fold cutoff used in Fig 2 since the magnitude of destabilization by Nos is generally smaller than the magnitude of degradation by Upf1-Nos. mRNAs stabilized or destabilized in the absence of Nos at an FDR < 0.05 are orange and blue, respectively. (**B**) The barcode shows mRNAs depleted by Upf1-Nos (Fig 2) plotted vs. the $\log_2$ (fold change) in *nos*⁻ vs. wt at 2–3 hours (e.g., Fig 6A). Each depleted mRNA is a hashmark, the length of which indicates the extent of depletion by Upf1-Nos; this plot shows a poor correlation between the extent of degradation by Upf1-Nos and by Nos in wt embryos (see also the scatterplot in D). (**C**) A Venn diagram shows that most of the maternal mRNAs stabilized in the absence of Nos are degraded by Upf1-Nos. (**D**) The scatterplot shows the correlation between the extent of degradation by Upf1-Nos and stabilization in the absence of Nos. The canonical Nos substrate *hb* mRNA is highlighted as an extreme example, in which zygotic reexpression between 2–3 hours almost completely obscures Nos-mediated regulation of maternal *hb* mRNA. In all these comparisons, we analyze only the 6,399 mRNAs common to the 2 datasets (e.g., Figs 2A and 6A). Underlying data for the figure are in S5 Data. FDR, false discovery rate; *hb*, *hunchback*; Nos, Nanos; wt, wild type.

https://doi.org/10.1371/journal.pbio.3002840.g006

therefore, essentially no zygotically reexpressed mRNAs will suffer regulation by Nos even if they might be susceptible. This is not a confounding issue for our analysis of Upf1-Nos activity, since mRNA was harvested before the onset of transcription. However, zygotic reexpression likely does mask regulation of mRNA stability by Nos, thereby accounting, at least in part, for the modest correlation between the extent of regulation by Upf1-Nos and by Nos ($R^2 = 0.25$; Fig 6D). For example, the canonical Nos target *hb* (highlighted in the scatter plot in Fig 6D), which is among the most sensitive Upf1-Nos targets, is retranscribed in the 2- to 3-hour window such that the net level of *hb* mRNA at 2 to 3 hours of development is not significantly different in the presence or absence of Nos.

To estimate the potential influence of zygotic reexpression on the 2- to 3-hour samples ± Nos, we first analyzed data from Lott and colleagues (see S5 Data) [54]. Their

measurements of RNA abundance in precisely staged single embryos allow us to determine the fraction of maternal mRNAs in our experiments that are reexpressed zygotically within 3 pools: mRNAs targeted by both Upf1-Nos and Nos (pool A; 105/1,019 = 10%); mRNAs targeted by Upf1-Nos but not Nos (pool B; 655/1,528 = 43%); and mRNAs targeted by neither (pool C; 760/3,852 = 20%). There is a striking enrichment of zygotically reexpressed mRNAs in pool B (p-values $< 2.2 \times 10^{-16}$ versus pools A or C, respectively, by Fisher exact test). Taken together, these observations support the idea that, for many of the genes in pool B, Nos-dependent degradation of the maternal mRNA component might be masked by new transcription at 2 to 3 hours of embryonic development (e.g., as for *hb*).

We reasoned that we might observe a reduction in poly(A) tail length and TE of the 1,528 mRNAs in pool B at earlier stages of development, before the potentially confounding contribution of zygotic transcription. To test the idea, we returned to the resource described by Eichhorn and colleagues [51], examining the fate of maternal mRNAs at various stages from late oogenesis through the first hour of embryonic development. Data were parsed into the 3 pools described above: (A) the 1,019 mRNAs targeted both by Upf1-Nos and Nos; (B) the 1,528 mRNAs targeted only by Upf1-Nos; and (C) the remaining 3,852 mRNAs not targeted by Upf1-Nos. As shown in Fig 7A, the 2 pools containing Upf1-Nos-targeted mRNAs (A and B) are regulated in a similar fashion, particularly at egg activation: mRNAs in both pools are translationally repressed and suffer shortening of their poly(A) tails (albeit, to slightly different extents; S5 Data). In contrast, the mRNAs not targeted by Upf1-Nos (pool C) are translationally activated and undergo lengthening of their poly(A) tails.

Overall, we conclude that, at or around the oocyte–egg transition, endogenous Nos likely regulates most of the maternal mRNAs targeted by Upf1-Nos.

Nos is a major contributor to maternal mRNA degradation in the early embryo

As in many organisms [56], a large proportion of the maternal transcriptome is degraded during early *Drosophila* embryonic development. Our analysis in Fig 5B suggests that mRNAs targeted by Upf1-Nos are degraded during the MZT. But we could not easily gauge the overall contribution of Upf1-Nos, or Nos, to maternal degradation in general from these data. We therefore turned to experiments in which maternal mRNA degradation has been measured more directly [55]. Thomsen and colleagues measured degradation in both unfertilized eggs and in embryos before and after onset of the MZT using microarrays. Their experiments reveal that 60% of maternal transcripts are degraded in the early embryo and that degradation of each mRNA is dependent on the activity of maternal factors, zygotic factors, or a mixture of the two. The initial wave of degradation has recently been verified via analysis of single embryo transcriptomes using RNAseq [57].

We asked whether the subsets of degraded maternal mRNAs and mRNAs targeted by Upf1-Nos overlap. The striking result is that 25% of degraded maternal mRNAs are targeted by Upf1-Nos and by Nos, and an additional 34% of degraded maternal mRNAs are targeted by Upf1-Nos but not Nos (S6 Data); conversely, the overwhelming majority of Upf1-Nos targets (90%) are degraded in wild-type embryos (Fig 7B). These observations support the ideas that (1) Nos contributes to the degradation of between 25% and 59% of maternal mRNAs in wild-type embryos and (2) Upf1-Nos does not adventitiously target otherwise stable mRNAs. Parsing the data of Thomsen and colleagues reveals that degradation of mRNAs targeted by both Upf1-Nos and Nos is dependent on both maternal and zygotic factors (Fig 7B). Their data further show that at least 19% of mRNAs targeted by Upf1-Nos but not Nos are zygotically

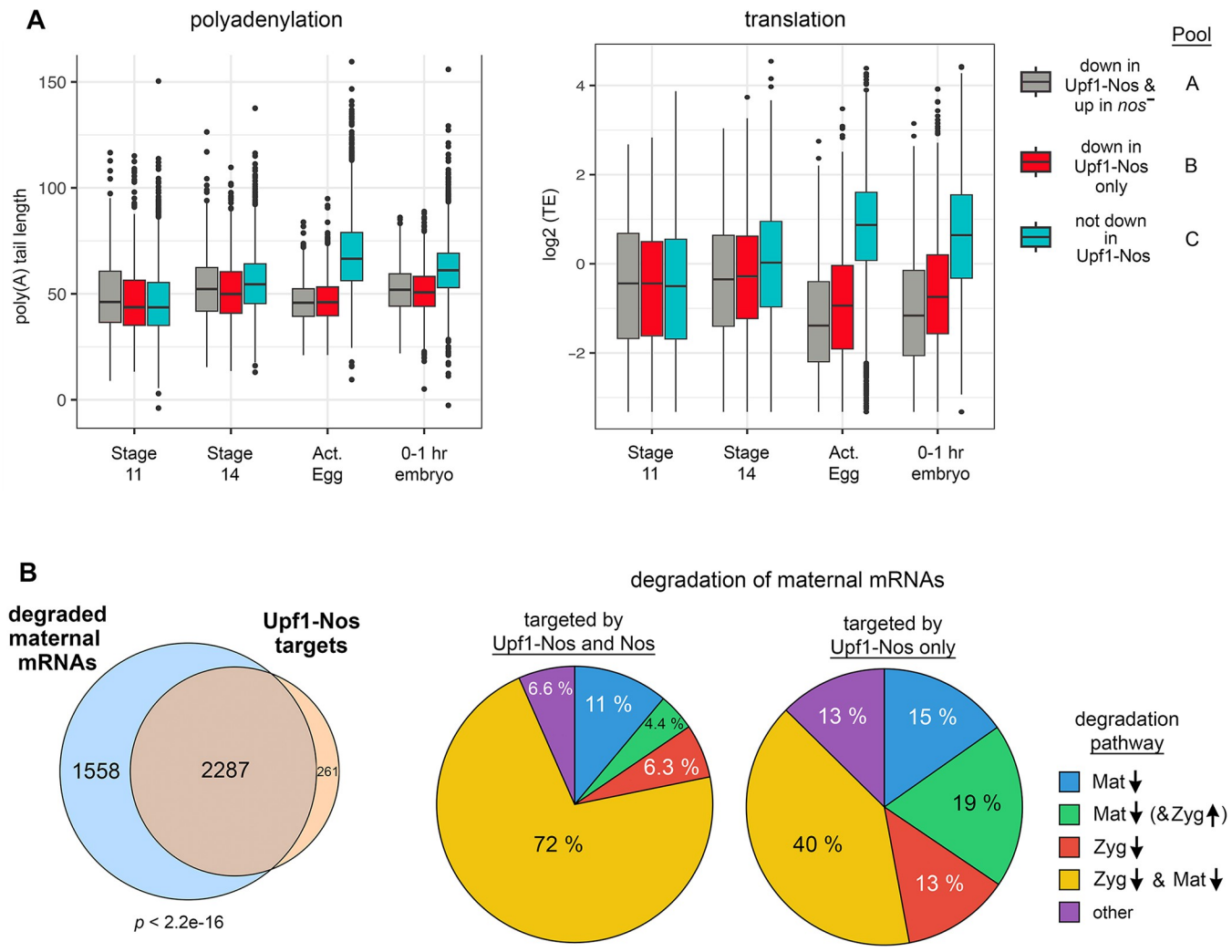

Fig 7. Regulation of maternal mRNA polyadenylation, translation, and degradation by Upf1-Nos and Nos. (**A**) Maternal mRNAs were divided into 3 pools: down in Upf1-Nos and up in *nos*⁻ at 2–3 hours (Pool A); down in Upf1-Nos only (Pool B); and the remaining 3,852 maternal mRNAs untargeted by Upf1-Nos (Pool C). These bins were used to parse the data of Eichhorn and colleagues [51], as described for Fig 5. Statistical analysis in S5 Data. (**B**) Analysis of unstable maternal mRNAs degraded in early embryogenesis. At the left is shown the overlap between maternal mRNAs that are degraded in the first 3 hours of embryogenesis (60% of all maternal mRNAs; [55]) with mRNAs targeted by Upf1-Nos. To the right are Venn diagrams showing the distribution of mRNAs among various degradation pathways. Down arrows denote degradation by either Mat or Zyg pathways, and the single upward arrow indicates zygotic reexpression. These correspond to mRNA classes II-V in [55] and an "other" category, which consists primarily of mRNAs absent from Thomsen and colleagues' data, as well as minor contributions from stable maternal mRNAs (class I) and purely zygotic mRNAs (class VII). Underlying data and statistical analysis in S6 Data. Mat, maternal; Nos, Nanos; Zyg, zygotic.

https://doi.org/10.1371/journal.pbio.3002840.g007

reexpressed (Fig 7B), supporting our idea that zygotic expression masks Nos-dependent degradation in the experiments of Fig 6.

Overall, we conclude that Nos regulates the poly-adenylation, translation, and stability of a large portion of the maternal transcriptome.

Discussion

The main conclusions from the work presented above are that Nos regulates thousands of mRNAs in the maternal transcriptome and likely does so in concert with Pum, binding jointly to NRE sequences much as they do to the NREs in *hb* mRNA. The latter idea is supported

primarily from the relative inactivity of Upf1-Nos^{L7}, which bears a defective C-terminal tail, a critical element of the intricate set of protein–protein and protein–RNA interactions that support formation of the Nos/Pum/*hb* NRE ternary complex [22]. In theory, the Nos C-terminal tail might mediate similar interactions with another RNA-binding partner too. Although we cannot rule out such an idea, the enrichment of NREs among mRNAs depleted by Upf1-Nos (Fig 3) or repressed at egg activation (presumably by endogenous Nos; Fig 5) supports the idea that most of the Nos tail-dependent activity is mediated via Pum as a partner.

A number of factors drove us at the outset to adopting the unconventional approach of using Upf1-Nos to identify Nos regulatory targets. First, we failed to achieve meaningful enrichment of *hb* mRNA in pulldown experiments from embryonic extracts expressing epitope-tagged Nos. This disappointing observation was mitigated by the modest enrichment of the canonical Nos+Pum targets *hb* or *bcd* mRNA in the Pum pulldown experiments of others [27,28]. In these experiments, *hb* and *bcd* mRNA were enriched only between 2- and 3.5-fold, even though Pum on its own is a high-affinity, high-specificity binding protein. Given the modest enrichment for known Pum-bound mRNA targets, the high nonspecific binding activity of Nos, and our insignificant enrichment of *hb* in pilot experiments, we were not encouraged to believe that we would be able to purify other, less stable Nos complexes formed on suboptimal NREs, for example. We also considered using UV-crosslinking to stabilize Nos/mRNA complexes in extracts, but crosslinking of the purified Nos RBD is inefficient [23]. In contrast, in vivo expression of Upf1-Nos allowed us to achieve high activity and specificity: *hb* and *bcd* are depleted 131- and 34-fold, respectively, by Upf1-Nos, whereas upon expression of Upf1-Nos^{L7} *hb* is depleted only 1.5-fold and the level of *bcd* is not significantly changed. The large dynamic range of our experiment allowed the identification of thousands of less-sensitive targets, and over 1,000 of these are verified by virtue of stabilization in the absence of Nos (Fig 6).

There are a number of caveats to our experiments. First, the Upf1-Nos chimera is overexpressed 3-fold (relative to endogenous Nos) and thus may target some mRNAs not usually regulated by Nos. Second, the irreversible degradation of targeted mRNAs by Upf1-Nos may capture weakly regulated targets, much as UV-crosslinking in CLIP experiments can capture transient, low affinity mRNA targets [58]. Third, we have not shown that mRNAs regulated by either Upf1-Nos or Nos in vivo are directly bound by Nos in vitro. And finally, we have not identified specific sites within regulated mRNAs that mediate Nos action.

Although we have not identified the sites within regulated mRNAs that mediate Nos (or Upf1-Nos) action, analysis of the population of targeted mRNAs has shown that Nos+Pum preferentially recognize mRNAs with both UGUU and UGUA motifs. We observe a correlation between the density of such motifs in the 3′ UTR and sensitivity to Upf1-Nos but have not been able to identify similar correlations between the total number of motifs or their position within the 3′ UTR. At one level, this is surprising, since a single site is sufficient to confer regulation either in flies or in cultured cells, and the degree of regulation correlates roughly with the number of sites [22,38]. Therefore, one might expect that mRNAs with many sites would be more sensitive, as the probability of occupancy by a Nos+Pum repressor complex would be greater. This is clearly not the case; for example, of the 10 mRNAs in the transcriptome with the largest number of 3′ UTR UGUA motifs [26], only one is targeted by Upf1-Nos. The correlation that we do observe (Fig 3C) is consistent with the idea that higher site density promotes cooperative interactions among nearby bound complexes. This model is supported by experiments described elsewhere showing that the N-terminal domain of Pum interacts with itself [42]. Finally, the contribution of other RNA-bound regulators or RNA structure is too complex to currently be taken into account when considering the entire transcriptome, as has been pointed out previously [26].

Given the large number of regulated mRNAs, it is not surprising that expression of Nos protein is tightly controlled. During oogenesis and embryogenesis, much of this control is exerted via the 3′ UTR of its mRNA to control the timing and location of protein accumulation [31,59,60]; we therefore intentionally designed all of the transgenes used in this work to express mRNAs bearing the native *nos* 3′ UTR. Our results suggest an additional level of control—negative autoregulation. Nos mRNA is significantly depleted (6.7-fold) by Upf1-Nos, and most of this regulation appears to be Pum-mediated (e.g., only 1.3-fold depletion by Upf1-Nos^{L7}). The idea of negative autoregulation is consistent with earlier work on the activity of Nos at the neuromuscular junction, which hinted at Pum-dependent autoregulation via noncanonical sites in the *nos* 3′ UTR [16].

Based initially on analysis of the low residual activity of Upf1-Nos^{L7}, we argue above that Bru may recruit Nos (or Nos^{L7}) to regulate a minor portion of the maternal transcriptome. Such a model could explain an intriguing aspect of Nos biology in the female germline stem cell and its progeny cystoblast, which differentiates into the cyst of 16 cells that ultimately forms the germline component of each egg chamber. In females bearing near-complete loss-of function *nos* alleles (e.g., *nos*^{RC}), GSCs are specified normally but fail to maintain stem cell status following division: Both daughter cells differentiate, and the ovary is rapidly denuded of its germline [61]. However, GSC function is maintained in the *nos*^{L7} mutant, suggesting that at least some of the essential Nos function at this stage is tail-independent and therefore not mediated by Pum [24]. Our results are consistent with the idea that Bru mediates part of the activity of Nos in early oogenesis and does so whether the Nos C-terminal tail is intact or not. Bru is required both in the larval ovary for normal development of the GSCs and in the adult ovary for the development of cystoblast progeny [62]. The definitive cellular marker for the GSC and the cystoblast is the spectrosome, an unusual intracellular sphere containing cytoskeletal proteins usually associated with the cellular membrane—alpha- and beta-spectrin, spectraplakin (which links actin and microtubule filaments), and an adducin (encoded by *hts*), which mediates interactions between spectrin and actin [63–65]. We find that the mRNAs encoding these proteins and functionally related cytoskeletal factors are enriched among Upf1-Nos^{L7} targets (Fig 4C). Taken together, these observations lead us to speculate that at least part of the function of Nos in maintaining stem cell identity in the GSCs may rely on Bru-mediated regulation of mRNAs encoding the spectrosome and other cytoskeletal components.

Part of the motivation for identifying novel Nos regulatory targets was the hope of gaining insight into its evolutionarily conserved role in the GSCs, where it maintains stem cell identity by incompletely defined pathways, and the PGCs, where it regulates proliferation, contributes to selectively blocking transcription of somatic genes and promotes escape from apoptosis. The *brat* and *Mei-P26* mRNAs are derepressed in *nos* mutant GSCs [66,67], suggesting they might be critical regulatory targets. However, in neither case has Nos been shown to bind to the mRNA nor have regulatory sites that mediate its action been ablated, thereby relieving repression. Interestingly, neither of these mRNAs is stabilized in the absence of Nos (Fig 6); *Mei-P26* mRNA is depleted only 3.3-fold by Upf1-Nos, and *brat* mRNA is not regulated by Upf1-Nos (S2 Data). Based on the large set of Nos targets we have identified, we suggest that Nos may directly regulate many other mRNAs to maintain GSCs, in contrast to the singular regulation of maternal *hb* mRNA that drives abdominal patterning in the embryo. Translation is globally repressed in human hematopoietic stem cells [68]; perhaps Nos-mediated global repression contributes to maintenance of a semidormant state that promotes GSC maintenance. Alternatively, targeting of particular pathways could regulate GSCs. For example, our finding that DNA replication gene mRNAs are preferentially targeted by Upf1-Nos might depress fork speed, which has recently been shown to promote a totipotent state in mouse embryonic stem cells [69].

The experiments described in Figs 6 and 7 reveal an unanticipated role for Nos in the degradation of thousands of maternal mRNAs in the embryo. Maternal mRNAs are first exposed to high levels of Nos and Pum in the nurse cell cytoplasm at stages 9 to 10B of oogenesis and remain exposed in the oocyte cytoplasm through stage 13 [31]. Taken together, our data are consistent with the idea that Nos+Pum bind maternal mRNA targets in late oogenesis, thereby recruiting the CCR4/NOT/deadenylase complex. Targeted mRNAs apparently remain hypoadenylated and translationally repressed through fertilization and egg activation (Fig 7), even though Nos is absent from most of the oocyte cytoplasm during the intervening approximately 2-hour period that constitutes oogenesis stage 14. The mechanism by which repression persists in the absence of high levels of Nos is unclear. One possibility is that activity of the ovarian cytoplasmic poly(A) polymerase (encoded by *wispy* in *Drosophila* [70,71]) is too low in late oogenesis to efficiently add poly(A) tails to such a large portion of the transcriptome. Another possibility is that, after initial recruitment to targeted mRNAs by Nos+Pum, binding of the CCR4 deadenylation complex is maintained during the (relatively brief) absence of Nos due to direct interactions with Pum [72] (or other, unknown RNA-bound factors). Upon egg activation, repressed mRNAs are degraded in the embryo, both by other maternal factors (such as Smg [50]; Fig 5A) and by zygotically expressed factors during the MZT (Fig 7B). These ideas are broadly consistent with the work of Eichhorn and colleagues [51], who concluded that poly(A) tail shortening rather than poly(A) lengthening plays the major role in setting relative poly(A) length and translational status of maternal mRNAs at egg activation.

The downstream developmental consequences of the Nos+Pum-dependent regulation we observe are unclear. The embryonic fate map and gene expression program are drastically altered in embryos that develop without a maternal endowment of Nos (or Pum), due to the suppression of abdominal segmentation. Further exploring the results of derepressing and stabilizing Nos mRNA targets in theory would be possible in embryos from germline clones lacking both *nos* and maternal *hb* function [13,14,34]. Such an experiment is likely to be technically challenging; to our knowledge, it has not been performed to test the role of other maternal factors, such as Pum or Brat, on the downstream effects of misregulating maternal mRNAs in the embryo.

We note that the (Nos+Pum)-dependent degradation of maternal mRNAs reported here appears to be distinct from the Pum-dependent degradation of maternal mRNAs that has previously been reported [28]. Laver and colleagues identified 641 mRNAs that bind Pum among a mixture of maternal and zygotic mRNAs in 0- to 3-hour embryo extracts. These only partially (47%) overlap with the set of ovarian mRNAs that bind Pum in the experiments of Gerber and colleagues [27] (analyzed in Fig 3A); in addition, they are not significantly enriched among mRNAs targeted by Upf1-Nos ($p = 0.98$ by the CAMERA competitive test; S10 Fig). The mRNAs identified by Laver and colleagues appear to bind Pum alone rather than Nos+Pum, as they are enriched for a quasi-canonical Pum motif rather than the Nos+Pum motif defined in vitro [22] or the variant we identify in Fig 3. Taken together, current data are consistent with 2 roles for Pum in degradation of distinct subsets of maternal mRNAs—the Nos-dependent function in late oogenesis described in this report and a Nos-independent function during the MZT in the 2- to 3-hour embryo.

In conclusion, Nos is responsible for regulating mRNA fate on 2 very different scales in the early embryo—repressing a single mRNA (*hb*) to govern abdominal segmentation and thousands of mRNAs to help direct turnover of the maternal transcriptome.

Materials and methods

Drosophila strains and methods

Plasmids used in this study are described in S7 Data. Transgenic lines were constructed by microinjection of w^{1118} embryos by standard methods. The following strains were used: w^{1118}

as the wild-type reference in RNAseq experiments; the maternal alpha-tubulin GAL4-VP16 driver (stock # 7062 from the Bloomington Drosophila Stock Center [BDSC]); *trans*-heterozygotes of nos^{BN} and Df(3R)Exel6183 (stock # 7662, [BDSC]) for the RNAseq experiment of Fig 6. We initially tested 3 or more transgenic lines with the GAL4-VP16 driver for each construct and observed only minor phenotypic differences among the 3 lines. We screened for lines expressing Upf1-Nos and Upf1-Nos^{L7} at essentially the same level by harvesting total RNA from collections of 0- to 2-hour embryos and measuring the chimeric mRNA by RT-qPCR using the appropriate primer pair in S2 Data. Fly stocks were maintained by standard methods and grown at 25˚C. Embryos were collected on apple juice agar plates smeared with yeast paste.

Early embryos for assessment of nuclear morphology (Fig 1) were prepared by dechorionating in bleach, harvesting by filtration, fixing in 4% formaldehyde under heptane for 20 to 30 minutes, removal of the aqueous phase and shocking into methanol. Embryos were then rehydrated into phosphate-buffered saline (PBS) containing 0.1% Tween-20 (PBT) and incubated with 5 μg/ml 4′,6-diamidino-2-phenylindole (DAPI) for 10 minutes, washed repeatedly with PBT, mounted in PBST containing 25% glycerol, and examined by epifluorescence using a Zeiss Axiophot.

Embryonic cuticle was examined by harvesting embryos from apple juice plates 24 hours after removing adults, dechorionating with bleach, and mounting in Hoyers/lactic acid. Slides were cleared by heating for several hours and then examined by dark field microscopy using a Zeiss Axiophot.

In situ hybridization was performed essentially as described [73], with probe prepared by nick translation of a double-stranded PCR product bearing the *bcd* ORF using alkali-stable digoxigenin-11-2′-deoxyuridine-5′-triphosphate (Roche), visualizing with alkaline-phosphate coupled sheep anti-digoxigenin Fab fragments (Roche) and subsequent reaction with 5-bromo-4-chloro-3-indolyl phosphate and nitro blue tetrazolium before examination using Nomarski optics on a Zeiss Axiophot.

For hand-sorting of embryos to identify those in nc 9 to 10, we followed the protocol of [74] with the following modifications. Embryos were dechorionated in 100% bleach for 1 minute, rinsed well, and then simultaneously devitellinized and fixed in a 1:1 ratio of ice-cold methanol and heptane for 5 minutes with gentle rocking. The vials were vortexed for 30 seconds, heptane and embryos at the interface removed, and the remaining embryos washed with ice-cold methanol 3 times. Embryos were then rehydrated into PBT with washing for 10 minutes and then stained with 0.1 μg/ml DAPI for 10 minutes. After washing in PBT, embryos were sorted under UV illumination using a Leica MZFLIII stereomicroscope.

For the western blot of S1 Fig, 0- to 2-hour embryo collections from transgenic females were homogenized in sample buffer and transferred to 0.2 μm nitrocellulose following SDS-PAGE. We analyzed samples from 2 independent transgenic HA-Nos and HA-Upf1-Nos lines. The influenza hemagglutinin (HA) epitope was detected with monoclonal C29F4 rabbit anti-HA (3274, Cell Signaling Technology) and the α-tubulin loading control with monoclonal B-5-1-2 (T5168, Sigma), followed by goat anti-rabbit IRDye 800 IgG secondary antibodies (LiCor 926–32211) and goat anti-mouse IRDye 680 IgG secondary antibodies (LiCor 926–68070), with detection and quantitation using a LI-COR Odyssey CLx.

RNAseq and RT-qPCR

Total RNA was extracted from sorted embryos using TRIzol reagent (Thermo Fisher Scientific). Samples were submitted to the Ohio State University Cancer Center Genomics Shared Resource for poly(A) selection and library preparation with TruSeq (Illumina) and

subsequently sequenced on a HiSeq4000 (Illumina) sequencer. Paired-end 150-nucleotide (nt) raw reads were first processed and demultiplexed at the sequencing facility and subsequently processed as follows. Adapter sequences were trimmed followed by trimming low-quality bases from the 3′ end of reads based on a minimum Phred score of 15. Reads of less than 60 nt were removed, as were reads mapping to mtRNA, tRNA, and rRNA. STAR (v2.5.3a) was used to map the reads either to the fly genome or the transcriptome [75]. Mapped reads were counted using RSEM (v1.3.0) [76]. The resulting outputs were analyzed in R (v4.2.1) using the edgeR package (v3.40.2) to find differentially expressed genes and transcripts [77]. Low abundance genes and transcripts were filtered out by setting min.count = 30 and min.total. count = 30 in filterByExpr function in the edgeR package, removing genes and transcripts with approximately <2 counts per million mapped reads. All statistical analyses including differential expression and locally estimated scatterplot smoothing (LOESS) were performed using R (v4.2.1). R code is available at https://zenodo.org/doi/10.5281/zenodo.13337141 with updates at https://github.com/marhabaie/dmel-nanos-targets.

To account for oversampling caused by the large depletion of mRNAs targeted by Upf1-Nos, correction factors for these data were calculated essentially as described [36]. We assumed that the most abundantly expressed mRNAs, which are transcribed from housekeeping genes, are not regulated by Upf1-Nos and thus can be used to calculate a correction factor. Rather than relying on a single highly expressed gene (e.g., eEF1α1), an average correction factor was calculated using the 20 most abundantly expressed genes for each Upf1-Nos replicate. Among genes with the highest average read abundance in wild type samples, we selected 20 with a similar rank order among Upf1-Nos and wild-type samples. For each gene, the ratio of read abundance in the Upf1-Nos replicate to its average abundance across the 3 wild-type replicates was calculated. The resulting ratios for all 20 genes were averaged, yielding a correction factor for the replicate (S2 Data). These correction factors were used as normalization factors for the Upf1-Nos replicates in edgeR. A similar approach was used to calculate 3 correction factors for the analysis of individual transcripts (S2 Data).

For RT-qPCR, cDNA was synthesized from 250 ng RNA using random hexamers and qPCR performed using SYBR Green using a 7500 Real Time PCR machine (Applied Biosystems). Triplicate measurements for each primer pair were obtained (for each of the 3 biological replicates). Abundance of each RT product was calculated relative to the abundance of RT product from RpS2 mRNA. Primer efficiencies for all primer pairs were 90% to 100%.

Motif enrichment analysis

Motif enrichment analysis was done using the following DREME command: "dreme -rna -norc -png -e 0.1 -m 10 -o DEOUT -p input.fa". Parameters were set per the user manual. To prevent outlier large 3′ UTRs (e.g., the approximately 10.5-kb *headcase* 3′ UTR) from biasing the analysis, only UTRs <2,600 nt (98% of all 3′ UTRs) were analyzed.

Gene ontology enrichment analysis

GO enrichment analysis was performed using DAVID (v6.8) with the default setting and categories (COG_ONTOLOGY, UP_KEYWORDS, UP_SEQ_FEATURE, GOTERM_BP_DIRECT, GOTERM_CC_DIRECT, GOTERM_MF_DIRECT, KEGG_PATHWAY, INTERPRO, SMART).

Yeast interaction assays

Yeast were transformed with the 2-μ plasmids described in S7 Data by a standard lithium acetate/PEG protocol. For 2-hybrid experiments, we used the PJ69-4A strain [78], which is

*MAT**a***, *trp1-901*, *leu2-3*, *112*, *ura3-52*, *his3-200*, *gal4Δ*, *gal80Δ*, *LYS2*::*GAL1-HIS3*, *GAL2-ADE2*, *met2*::*GAL7-lacZ*. Double transformants were obtained and grown on minimal SD dropout medium lacking tryptophan and leucine. For 3- and 4-hybrid experiments, we used the YBZ1 strain [79], which is *MAT**a***, *ura3-52*, *leu2-3*, *112*, *his3-200*, *trp1-1*, *ade2*, *LYS2*::*(LexAop)-HIS3*, *ura3*::*(lexA-op)-lacZ*, *LexA-MS2 coat (N55K)*. For 3-hybrid experiments, double transformants were grown on minimal SD dropout medium lacking uracil and leucine, and for 4-hybrid experiments, triple transformants were grown on SD dropout medium lacking uracil, leucine, and tryptophan.

β-galactosidase activity was measured using Beta-Glo (Promega) essentially as described [79]. Briefly, transformants were grown by diluting saturated overnight cultures into appropriate selective media to early-log phase (OD_{600} = 0.2 to 0.3), and then 40 μl of culture was incubated with the same volume of Beta-Glo reagent for 60 minutes at room temperature in 96-well microplates. Three transformants were grown separately and assayed for each experiment. Samples were analyzed in a Veritas luminometer (Turner Biosystems). The output signal from the luminometer was divided by the OD_{600} to normalize for the number of cells in each sample, and by 1,000 (by convention) to generate a reading of beta-galactosidase activity in arbitrary light units.

Supporting information

S1 Fig. (Related to Fig 1). Western blot showing expression of HA-tagged Upf1-Nos and HA-tagged Nos in 0–2-hour embryos. Quantitation is in S1 Data. The first lane is from non-transgenic *w* embryos and the loading control is alpha-tubulin. MW markers in kDa to the left. Underlying data are in S1 Data.
(PDF)

S2 Fig. (Related to Fig 2). Multidimensional scaling plot of RNAseq data in Fig 2. Underlying data are in S2 Data.
(PDF)

S3 Fig. (Related to Fig 2). Smear plots of the RNAseq data plotted for individual mRNAs rather than gene-binned mRNAs (as in Fig 2A). Underlying data are in S2 Data.
(PDF)

S4 Fig. (Related to Fig 2). Smear plot displaying relative mRNA levels in Upf1-Nos vs. wt without adjustment for oversampling of unregulated mRNAs. As in Fig 2, the fractions of mRNAs significantly up- and down-regulated are in green to the right. Underlying data are in S2 Data.
(PDF)

S5 Fig. (Related to Fig 2). Boxplot showing that mRNAs targeted by Upf1-Nos have, on average, slightly shorter 3′ UTRs than nontargeted mRNAs. Underlying data are in S2 Data.
(PDF)

S6 Fig. (Related to Fig 3). Localized regression of the data analyzed in Fig 3C. Figure shows the density of NRE variants at position +4 in 3′ UTR sequence plotted against the $\log_2$ (fold change) in Upf1-Nos vs. wt. Each curve is labelled by the identity of the nucleotide at position +4 in the NRE (i.e., "U/A" corresponds to $\frac{U}{A}\frac{U}{A}\frac{U}{A}UGU\frac{U}{A}$). Here and in the LOESS analyses of Figs 5C and S7, the x-axis is nonlinear, light shading marks 95% confidence windows, the light dashed line marks $\log_2 = 0$, and the heavier dashed line marks $\log_2 \pm 1$. Underlying data are in S2 Data.
(PDF)

S7 Fig. (Related to Fig 4). Localized regression of the data analyzed in Fig 4A. Underlying data are in S2 Data.
(PDF)

S8 Fig. (Related to Fig 4). Barcode plot showing no significant enrichment of mRNAs targeted by Upf1-Nos among Bru-repressed mRNAs. Underlying data are in S2 Data.
(PDF)

S9 Fig. (Related to Fig 5). Bar graph showing enrichment in the density (sites/kb of 3′ UTR on the y-axis) of the 3 motifs shown above in translationally repressed mRNAs (negative vs. positive TE), with *p*-values calculated in the Wilcoxon test. Figure is a LOESS analysis of the data shown in Fig 5C. Underlying data are in S4 Data.
(PDF)

S10 Fig. (Related to Figs 3 and 7). Barcode plot showing no significant enrichment among mRNAs depleted by Upf1-Nos of mRNAs bound by Pum in 0–3-hour embryonic extracts identified by Laver and colleagues. Zygotically expressed mRNAs in their data were omitted from the analysis. Underlying data are in S2 Data.
(PDF)

S1 Data. Underlying data for Figs 1B and S1.
(XLSX)

S2 Data. Underlying data for Figs 2, S2–S8 and S10.
(XLSX)

S3 Data. Underlying data for Fig 4.
(XLSX)

S4 Data. Underlying data for Figs 5 and S9.
(XLSX)

S5 Data. Underlying data for Fig 6.
(XLSX)

S6 Data. Underlying data for Fig 7.
(XLSX)

S7 Data. Plasmids used in this work.
(XLSX)

S1 Raw Images. S1 Fig raw image.
(TIF)

Acknowledgments

We thank Drs. K Panda, RK Slotkin, and R Bundschuh for advice and helpful discussions; Dr. P Yan for assistance with RNAseq sample preparation; Drs. G Singh and M Kearse for comments on the manuscript; Dr. H Lipshitz for kindly forwarding their data for analysis in Fig 5A; Drs. E P-Mojica and H Lempradl for forwarding the data of Thomsen and colleagues for analysis in Fig 7B; and Dr. C Croce for encouragement and support. We acknowledge services of the OSUCCC Genomics Shared Resource, which is supported by P30CA016058. Some fly stocks were obtained from the Bloomington Drosophila Stock Center (NIH P40OD018537).

Author Contributions

Conceptualization: Mohammad Marhabaie, Tammy H. Wharton, Robin P. Wharton.

Data curation: Mohammad Marhabaie, Tammy H. Wharton, Sung Yun Kim, Robin P. Wharton.

Formal analysis: Mohammad Marhabaie, Sung Yun Kim, Robin P. Wharton.

Funding acquisition: Robin P. Wharton.

Investigation: Mohammad Marhabaie, Tammy H. Wharton, Sung Yun Kim, Robin P. Wharton.

Methodology: Mohammad Marhabaie.

Project administration: Robin P. Wharton.

Resources: Robin P. Wharton.

Supervision: Robin P. Wharton.

Validation: Mohammad Marhabaie, Sung Yun Kim.

Writing – original draft: Robin P. Wharton.

Writing – review & editing: Mohammad Marhabaie, Tammy H. Wharton, Robin P. Wharton.

References

1. Kadyrova LY, Habara Y, Lee TH, Wharton RP. Translational control of maternal Cyclin B mRNA by Nanos in the Drosophila germline. Development (Cambridge, England). 2007; 134:1519–1527. https://doi.org/10.1242/dev.002212 PMID: 17360772
2. Raisch T, Bhandari D, Sabath K, Helms S, Valkov E, Weichenrieder O, et al. Distinct modes of recruitment of the CCR4-NOT complex by Drosophila and vertebrate Nanos. EMBO J. 2016; 35:974–990. https://doi.org/10.15252/embj.201593634 PMID: 26968986
3. Kusz-Zamelczyk K, Sajek M, Spik A, Glazar R, Jędrzejczak P, Latos-Bieleńska A, et al. Mutations of NANOS1, a human homologue of the Drosophila morphogen, are associated with a lack of germ cells in testes or severe oligo-astheno-teratozoospermia. J Med Genet. 2013; 50:187–193. https://doi.org/10.1136/jmedgenet-2012-101230 PMID: 23315541
4. Tsuda M, Sasaoka Y, Kiso M, Abe K, Haraguchi S, Kobayashi S, et al. Conserved role of nanos proteins in germ cell development. Science. 2003; 301:1239–1241. https://doi.org/10.1126/science.1085222 PMID: 12947200
5. Wang Z, Lin H. Nanos maintains germline stem cell self-renewal by preventing differentiation. Science. 2004; 303:2016–2019. https://doi.org/10.1126/science.1093983 PMID: 14976263
6. Asaoka M, Sano H, Obara Y, Kobayashi S. Maternal Nanos regulates zygotic gene expression in germline progenitors of Drosophila melanogaster. Mech Dev. 1998; 78:153–158. https://doi.org/10.1016/s0925-4773(98)00164-6 PMID: 9858716
7. Asaoka-Taguchi M, Yamada M, Nakamura A, Hanyu K, Kobayashi S. Maternal Pumilio acts together with Nanos in germline development in Drosophila embryos. Nat Cell Biol. 1999; 1:431–437. https://doi.org/10.1038/15666 PMID: 10559987
8. Kobayashi S, Yamada M, Asaoka M, Kitamura T. Essential role of the posterior morphogen nanos for germline development in Drosophila. Nature. 1996; 380:708–711. https://doi.org/10.1038/380708a0 PMID: 8614464
9. Sato K, Hayashi Y, Ninomiya Y, Shigenobu S, Arita K, Mukai M, et al. Maternal Nanos represses hid/skl-dependent apoptosis to maintain the germ line in Drosophila embryos. Proc Natl Acad Sci U S A. 2007; 104:7455–7460. https://doi.org/10.1073/pnas.0610052104 PMID: 17449640
10. Lee C-YS, Lu T, Seydoux G. Nanos promotes epigenetic reprograming of the germline by down-regulation of the THAP transcription factor LIN-15B. eLife. 2017:6. https://doi.org/10.7554/eLife.30201 PMID: 29111977

11. Subramaniam K, Seydoux G. nos-1 and nos-2, two genes related to Drosophila nanos, regulate primordial germ cell development and survival in Caenorhabditis elegans. Development (Cambridge, England). 1999; 126:4861–4871. https://doi.org/10.1242/dev.126.21.4861 PMID: 10518502

12. Hülskamp M, Schröder C, Pfeifle C, Jäckle H, Tautz D. Posterior segmentation of the Drosophila embryo in the absence of a maternal posterior organizer gene. Nature. 1989; 338:629–632. https://doi.org/10.1038/338629a0 PMID: 2704418

13. Irish V, Lehmann R, Akam M. The Drosophila posterior-group gene nanos functions by repressing hunchback activity. Nature. 1989; 338:646–648. https://doi.org/10.1038/338646a0 PMID: 2704419

14. Struhl G. Differing strategies for organizing anterior and posterior body pattern in Drosophila embryos. Nature. 1989; 338:741–744. https://doi.org/10.1038/338741a0 PMID: 2716822

15. Brechbiel JL, Gavis ER. Spatial regulation of nanos is required for its function in dendrite morphogenesis. Curr Biol. 2008; 18:745–750. https://doi.org/10.1016/j.cub.2008.04.033 PMID: 18472422

16. Menon KP, Andrews S, Murthy M, Gavis ER, Zinn K. The translational repressors Nanos and Pumilio have divergent effects on presynaptic terminal growth and postsynaptic glutamate receptor subunit composition. J Neurosci. 2009; 29:5558–5572. https://doi.org/10.1523/JNEUROSCI.0520-09.2009 PMID: 19403823

17. Ye B, Petritsch C, Clark IE, Gavis ER, Jan LY, Jan YN. Nanos and Pumilio are essential for dendrite morphogenesis in Drosophila peripheral neurons. Curr Biol. 2004; 14:314–321. https://doi.org/10.1016/j.cub.2004.01.052 PMID: 14972682

18. Coux R-X, Teixeira FK, Lehmann R. L(3)mbt and the LINT complex safeguard cellular identity in the Drosophila ovary. Development (Cambridge, England). 2018:145. https://doi.org/10.1242/dev.160721 PMID: 29511022

19. Janic A, Mendizabal L, Llamazares S, Rossell D, Gonzalez C. Ectopic expression of germline genes drives malignant brain tumor growth in Drosophila. Science. 2010; 330:1824–1827. https://doi.org/10.1126/science.1195481 PMID: 21205669

20. Miles WO, Korenjak M, Griffiths LM, Dyer MA, Provero P, Dyson NJ. Post-transcriptional gene expression control by NANOS is up-regulated and functionally important in pRb-deficient cells. EMBO J. 2014; 33:2201–2215. https://doi.org/10.15252/embj.201488057 PMID: 25100735

21. Curtis D, Treiber DK, Tao F, Zamore PD, Williamson JR, Lehmann R. A CCHC metal-binding domain in Nanos is essential for translational regulation. EMBO J. 1997; 16:834–843. https://doi.org/10.1093/emboj/16.4.834 PMID: 9049312

22. Weidmann CA, Qiu C, Arvola RM, Lou T-F, Killingsworth J, Campbell ZT, et al. Drosophila Nanos acts as a molecular clamp that modulates the RNA-binding and repression activities of Pumilio. eLife. 2016; 5:e17096. https://doi.org/10.7554/eLife.17096 PMID: 27482653

23. Sonoda J, Wharton RP. Recruitment of Nanos to hunchback mRNA by Pumilio. Genes Dev. 1999; 13:2704–2712. https://doi.org/10.1101/gad.13.20.2704 PMID: 10541556

24. Wang C, Dickinson LK, Lehmann R. Genetics of nanos localization in Drosophila. Dev Dyn Off Publ Am Assoc Anat. 1994; 199:103–115. https://doi.org/10.1002/aja.1001990204 PMID: 7515724

25. Wharton RP, Sonoda J, Lee T, Patterson M, Murata Y. The Pumilio RNA-binding domain is also a translational regulator. Mol Cell. 1998; 1:863–872. https://doi.org/10.1016/s1097-2765(00)80085-4 PMID: 9660969

26. Arvola RM, Weidmann CA, Tanaka Hall TM, Goldstrohm AC. Combinatorial control of messenger RNAs by Pumilio, Nanos and Brain Tumor Proteins. RNA Biol. 2017; 14:1445–1456. https://doi.org/10.1080/15476286.2017.1306168 PMID: 28318367

27. Gerber AP, Luschnig S, Krasnow MA, Brown PO, Herschlag D. Genome-wide identification of mRNAs associated with the translational regulator PUMILIO in Drosophila melanogaster. Proc Natl Acad Sci U S A. 2006; 103:4487–4492. https://doi.org/10.1073/pnas.0509260103 PMID: 16537387

28. Laver JD, Li X, Ray D, Cook KB, Hahn NA, Nabeel-Shah S, et al. Brain tumor is a sequence-specific RNA-binding protein that directs maternal mRNA clearance during the Drosophila maternal-to-zygotic transition. Genome Biol. 2015; 16:94. https://doi.org/10.1186/s13059-015-0659-4 PMID: 25962635

29. Lykke-Andersen J, Shu MD, Steitz JA. Communication of the position of exon-exon junctions to the mRNA surveillance machinery by the protein RNPS1. Science. 2001; 293:1836–1839. https://doi.org/10.1126/science.1062786 PMID: 11546874

30. Nott A, Le Hir H, Moore MJ. Splicing enhances translation in mammalian cells: an additional function of the exon junction complex. Genes Dev. 2004; 18:210–222. https://doi.org/10.1101/gad.1163204 PMID: 14752011

31. Forrest KM, Clark IE, Jain RA, Gavis ER. Temporal complexity within a translational control element in the nanos mRNA. Development (Cambridge, England). 2004; 131:5849–5857. https://doi.org/10.1242/dev.01460 PMID: 15525666

32. Li Y, Minor NT, Park JK, McKearin DM, Maines JZ. Bam and Bgcn antagonize Nanos-dependent germline stem cell maintenance. Proc Natl Acad Sci U S A. 2009; 106:9304–9309. https://doi.org/10.1073/pnas.0901452106 PMID: 19470484

33. Gavis ER, Lehmann R. Localization of nanos RNA controls embryonic polarity. Cell. 1992; 71:301–313. https://doi.org/10.1016/0092-8674(92)90358-j PMID: 1423595

34. Hülskamp M, Pfeifle C, Tautz D. A morphogenetic gradient of hunchback protein organizes the expression of the gap genes Krüppel and knirps in the early Drosophila embryo. Nature. 1990; 346:577–580. https://doi.org/10.1038/346577a0 PMID: 2377231

35. Wharton RP, Struhl G. Structure of the Drosophila BicaudalD protein and its role in localizing the posterior determinant nanos. Cell. 1989; 59:881–892. https://doi.org/10.1016/0092-8674(89)90611-9 PMID: 2590944

36. Risso D, Ngai J, Speed TP, Dudoit S. Normalization of RNA-seq data using factor analysis of control genes or samples. Nat Biotechnol. 2014; 32:896–902. https://doi.org/10.1038/nbt.2931 PMID: 25150836

37. Asaoka M, Hanyu-Nakamura K, Nakamura A, Kobayashi S. Maternal Nanos inhibits Importin-α2/Pendulin-dependent nuclear import to prevent somatic gene expression in the Drosophila germline. PLoS Genet. 2019; 15:e1008090. https://doi.org/10.1371/journal.pgen.1008090 PMID: 31091233

38. Wharton RP, Struhl G. RNA regulatory elements mediate control of Drosophila body pattern by the posterior morphogen nanos. Cell. 1991; 67:955–967. https://doi.org/10.1016/0092-8674(91)90368-9 PMID: 1720354

39. Huang DW, Sherman BT, Lempicki RA. Systematic and integrative analysis of large gene lists using DAVID bioinformatics resources. Nat Protoc. 2009; 4:44–57. https://doi.org/10.1038/nprot.2008.211 PMID: 19131956

40. Huang DW, Sherman BT, Lempicki RA. Bioinformatics enrichment tools: paths toward the comprehensive functional analysis of large gene lists. Nucleic Acids Res. 2009; 37:1–13. https://doi.org/10.1093/nar/gkn923 PMID: 19033363

41. Wu D, Smyth GK. Camera: a competitive gene set test accounting for inter-gene correlation. Nucleic Acids Res. 2012; 40:e133. https://doi.org/10.1093/nar/gks461 PMID: 22638577

42. Wharton TH, Marhabaie M, Wharton RP. Significant roles in RNA-binding for the amino-terminal domains of Drosophila Pumilio and Nanos. BioRxiv [Preprint]. 2023. https://doi.org/10.1101/2023.10.24.563753 PMID: 37961211

43. Flora P, Wong-Deyrup SW, Martin ET, Palumbo RJ, Nasrallah M, Oligney A, et al. Sequential Regulation of Maternal mRNAs through a Conserved cis-Acting Element in Their 3' UTRs. Cell Rep. 2018; 25:3828–3843.e9. https://doi.org/10.1016/j.celrep.2018.12.007 PMID: 30590052

44. Bailey TL. DREME: motif discovery in transcription factor ChIP-seq data. Bioinforma Oxf Engl. 2011; 27:1653–1659. https://doi.org/10.1093/bioinformatics/btr261 PMID: 21543442

45. Kim-Ha J, Kerr K, Macdonald PM. Translational regulation of oskar mRNA by bruno, an ovarian RNA-binding protein, is essential. Cell. 1995; 81:403–412. https://doi.org/10.1016/0092-8674(95)90393-3 PMID: 7736592

46. Reveal B, Garcia C, Ellington A, Macdonald PM. Multiple RNA binding domains of Bruno confer recognition of diverse binding sites for translational repression. RNA Biol. 2011; 8:1047–1060. https://doi.org/10.4161/rna.8.6.17542 PMID: 21955496

47. Bansal P, Madlung J, Schaaf K, Macek B, Bono F. An Interaction Network of RNA-Binding Proteins Involved in Drosophila Oogenesis. Mol Cell Proteomics. 2020; 19:1485–1502. https://doi.org/10.1074/mcp.RA119.001912 PMID: 32554711

48. Sonoda J. Combinatorial Translational Regulators in *Drosophila*. Ph.D., Duke University. 2001.

49. Verrotti AC, Wharton RP. Nanos interacts with cup in the female germline of Drosophila. Development (Cambridge, England). 2000; 127:5225–5232. https://doi.org/10.1242/dev.127.23.5225 PMID: 11060247

50. Tadros W, Goldman AL, Babak T, Menzies F, Vardy L, Orr-Weaver T, et al. SMAUG is a major regulator of maternal mRNA destabilization in Drosophila and its translation is activated by the PAN GU kinase. Dev Cell. 2007; 12:143–155. https://doi.org/10.1016/j.devcel.2006.10.005 PMID: 17199047

51. Eichhorn SW, Subtelny AO, Kronja I, Kwasnieski JC, Orr-Weaver TL, Bartel DP. mRNA poly(A)-tail changes specified by deadenylation broadly reshape translation in Drosophila oocytes and early embryos. eLife. 2016; 5:e16955. https://doi.org/10.7554/eLife.16955 PMID: 27474798

52. Dalby B, Glover DM. Discrete sequence elements control posterior pole accumulation and translational repression of maternal cyclin B RNA in Drosophila. EMBO J. 1993; 12:1219–1227. https://doi.org/10.1002/j.1460-2075.1993.tb05763.x PMID: 8458334

53. Tautz D. Regulation of the Drosophila segmentation gene hunchback by two maternal morphogenetic centres. Nature. 1988; 332:281–284. https://doi.org/10.1038/332281a0 PMID: 2450283

54. Lott SE, Villalta JE, Schroth GP, Luo S, Tonkin LA, Eisen MB. Noncanonical compensation of zygotic X transcription in early Drosophila melanogaster development revealed through single-embryo RNA-seq. PLoS Biol. 2011; 9:e1000590. https://doi.org/10.1371/journal.pbio.1000590 PMID: 21346796

55. Thomsen S, Anders S, Janga SC, Huber W, Alonso CR. Genome-wide analysis of mRNA decay patterns during early Drosophila development. Genome Biol. 2010; 11:R93. https://doi.org/10.1186/gb-2010-11-9-r93 PMID: 20858238

56. Tadros W, Lipshitz HD. The maternal-to-zygotic transition: a play in two acts. Development (Cambridge, England). 2009; 136:3033–3042. https://doi.org/10.1242/dev.033183 PMID: 19700615

57. Pérez-Mojica JE, Enders L, Walsh J, Lau KH, Lempradl A. Continuous transcriptome analysis reveals novel patterns of early gene expression in Drosophila embryos. Cell Genomics. 2023; 3:100265. https://doi.org/10.1016/j.xgen.2023.100265 PMID: 36950383

58. Chakrabarti AM, Haberman N, Praznik A, Luscombe NM, Ule J. Data Science Issues in Studying Protein-RNA Interactions with CLIP Technologies. Annu Rev Biomed Data Sci. 2018; 1:235–261. https://doi.org/10.1146/annurev-biodatasci-080917-013525 PMID: 37123514

59. Pekovic F, Rammelt C, Kubíková J, Metz J, Jeske M, Wahle E. RNA binding proteins Smaug and Cup induce CCR4-NOT-dependent deadenylation of the nanos mRNA in a reconstituted system. Nucleic Acids Res. 2023; 51:3950–3970. https://doi.org/10.1093/nar/gkad159 PMID: 36951092

60. Peng Y, Gavis ER. The Drosophila hnRNP F/H homolog Glorund recruits dFMRP to inhibit nanos translation elongation. Nucleic Acids Res. 2022; 50:7067–7083. https://doi.org/10.1093/nar/gkac500 PMID: 35699205

61. Forbes A, Lehmann R. Nanos and Pumilio have critical roles in the development and function of Drosophila germline stem cells. Development (Cambridge, England). 1998; 125:679–690. https://doi.org/10.1242/dev.125.4.679 PMID: 9435288

62. Parisi MJ, Deng W, Wang Z, Lin H. The arrest gene is required for germline cyst formation during Drosophila oogenesis. Genes N Y N. 2000; 2001(29):196–209. https://doi.org/10.1002/gene.1024 PMID: 11309853

63. de Cuevas M, Lee JK, Spradling AC. alpha-spectrin is required for germline cell division and differentiation in the Drosophila ovary. Development (Cambridge, England). 1996; 122:3959–3968. https://doi.org/10.1242/dev.122.12.3959 PMID: 9012516

64. Lin H, Yue L, Spradling AC. The Drosophila fusome, a germline-specific organelle, contains membrane skeletal proteins and functions in cyst formation. Development (Cambridge, England). 1994; 120:947–956. https://doi.org/10.1242/dev.120.4.947 PMID: 7600970

65. Röper K, Brown NH. A spectraplakin is enriched on the fusome and organizes microtubules during oocyte specification in Drosophila. Curr Biol. 2004; 14:99–110. PMID: 14738730

66. Harris RE, Pargett M, Sutcliffe C, Umulis D, Ashe HL. Brat promotes stem cell differentiation via control of a bistable switch that restricts BMP signaling. Dev Cell. 2011; 20:72–83. https://doi.org/10.1016/j.devcel.2010.11.019 PMID: 21238926

67. Joly W, Chartier A, Rojas-Rios P, Busseau I, Simonelig M. The CCR4 deadenylase acts with Nanos and Pumilio in the fine-tuning of Mei-P26 expression to promote germline stem cell self-renewal. Stem Cell Rep. 2013; 1:411–424. https://doi.org/10.1016/j.stemcr.2013.09.007 PMID: 24286029

68. Signer RAJ, Magee JA, Salic A, Morrison SJ. Haematopoietic stem cells require a highly regulated protein synthesis rate. Nature. 2014; 509:49–54. https://doi.org/10.1038/nature13035 PMID: 24670665

69. Nakatani T, Lin J, Ji F, Ettinger A, Pontabry J, Tokoro M, et al. DNA replication fork speed underlies cell fate changes and promotes reprogramming. Nat Genet. 2022; 54:318–327. https://doi.org/10.1038/s41588-022-01023-0 PMID: 35256805

70. Benoit P, Papin C, Kwak JE, Wickens M, Simonelig M. PAP- and GLD-2-type poly(A) polymerases are required sequentially in cytoplasmic polyadenylation and oogenesis in Drosophila. Development (Cambridge, England). 2008; 135:1969–1979. https://doi.org/10.1242/dev.021444 PMID: 18434412

71. Cui J, Sackton KL, Horner VL, Kumar KE, Wolfner MF. Wispy, the Drosophila homolog of GLD-2, is required during oogenesis and egg activation. Genetics. 2008; 178:2017–2029. https://doi.org/10.1534/genetics.107.084558 PMID: 18430932

72. Haugen RJ, Arvola RM, Connacher RP, Roden RT, Goldstrohm AC. A conserved domain of Drosophila RNA-binding protein Pumilio interacts with multiple CCR4-NOT deadenylase complex subunits to repress target mRNAs. J Biol Chem. 2022; 298:102270. https://doi.org/10.1016/j.jbc.2022.102270 PMID: 35850301

73. Tautz D, Pfeifle C. A non-radioactive in situ hybridization method for the localization of specific RNAs in Drosophila embryos reveals translational control of the segmentation gene hunchback. Chromosoma. 1989; 98:81–85. https://doi.org/10.1007/BF00291041 PMID: 2476281

74. Edgar BA, Sprenger F, Duronio RJ, Leopold P, O'Farrell PH. Distinct molecular mechanism regulate cell cycle timing at successive stages of Drosophila embryogenesis. Genes Dev. 1994; 8:440–452. https://doi.org/10.1101/gad.8.4.440 PMID: 7510257

75. Dobin A, Davis CA, Schlesinger F, Drenkow J, Zaleski C, Jha S, et al. STAR: ultrafast universal RNA-seq aligner. Bioinforma Oxf Engl. 2013; 29:15–21. https://doi.org/10.1093/bioinformatics/bts635 PMID: 23104886

76. Li B, Dewey CN. RSEM: accurate transcript quantification from RNA-Seq data with or without a reference genome. BMC Bioinformatics. 2011; 12:323. https://doi.org/10.1186/1471-2105-12-323 PMID: 21816040

77. Robinson MD, McCarthy DJ, Smyth GK. edgeR: a Bioconductor package for differential expression analysis of digital gene expression data. Bioinforma Oxf Engl. 2010; 26:139–140. https://doi.org/10.1093/bioinformatics/btp616 PMID: 19910308

78. James P, Halladay J, Craig EA. Genomic libraries and a host strain designed for highly efficient two-hybrid selection in yeast. Genetics. 1996; 144:1425–1436. https://doi.org/10.1093/genetics/144.4.1425 PMID: 8978031

79. Hook B, Bernstein D, Zhang B, Wickens M. RNA-protein interactions in the yeast three-hybrid system: affinity, sensitivity, and enhanced library screening. RNA N Y N. 2005; 11:227–233. https://doi.org/10.1261/rna.7202705 PMID: 15613539